

Theory of wakefields in a dielectric-lined waveguide

S. Y. Park* and J. L. Hirshfield†

*Department of Physics, Yale University, P.O. Box 208120, New Haven, Connecticut 06520-8120
and Omega-P, Incorporated, Suite 100, 345 Whitney Avenue, New Haven, Connecticut 06511*

(Received 18 February 2000)

Excitation of wakefields from a short charge bunch moving parallel to the axis of a dielectric-lined cylindrical waveguide is analyzed. This situation amounts to generation of Cerenkov radiation in a transversely bounded system. Wakefields are expanded into an orthonormal set of hybrid electric-magnetic eigenfunctions for this waveguide geometry. The orthonormalization relations for this system are obtained, evidently for the first time, both for a stationary source and for a localized moving source such as a charge bunch; it is shown that these orthonormalization relations differ. Forces arising from wakefields are found, valid within and behind a distributed bunch. Deviation of bunch distribution from axisymmetry leads to generation of dipole modes of significant amplitude that may lead to instability. Poynting's theorem is examined for this system, and it is shown that convected Coulomb field energy must be subtracted from the Poynting flux to obtain the radiation power. This power, which balances drag on the bunch as calculated directly from the fields, is shown to flow in a direction opposite to that of the charge bunch. The results are easily generalized to bunches of arbitrary length and charge distribution, and to a train of such bunches. Numerical examples are presented for monopole, dipole, and quadrupole wakefield forces, and sample electric field patterns are shown to assist in understanding the unusual nature of this type of Cerenkov radiation. For a 2-nC rectangular drive bunch of length 0.20 mm, moving along the axis of an alumina-lined waveguide ($\epsilon=9.50$) with inner and outer radii of 0.50 and 5.0 mm, a peak accelerating gradient behind the bunch of 155 MeV/m is predicted. This relatively high magnitude of accelerating gradient suggests that a simple uniform dielectric pipe could be the basis for the structure of a future high-gradient electron/positron linear accelerator, once low-emittance, kiloampere, subpicosecond electron bunches are available in the laboratory.

PACS number(s): 41.60.Cr, 41.75.Ht, 29.17.+w

I. INTRODUCTION

In 1997, a new approach was described for electron acceleration in the composite wakefield excited in a dielectric-lined waveguide by the passage of a finite periodic train of drive bunches [1]. The novelty of this approach rested upon two main features. *First*, the use of relatively short drive bunches was shown to allow the excitation of a large number of high-amplitude TM_{0m} waveguide modes in formation of the wakefields. The excited higher-order modes, with phase velocities equal to the bunch velocity and to one another, have nearly equally spaced eigenfrequencies. This leads to a strongly peaked spatiotemporal superposition of fields, with a net wakefield amplitude that can be much larger than the amplitudes of individual modes. The number of participating waveguide modes and the resulting peak intensity of the wakefield both increase as the bunch length decreases. Long bunches, as employed by others [2], cannot excite wakefields with peak amplitudes as large as short bunches carrying the same charge in the same structure. *Second*, the waveguide design can be such that these nearly periodic strongly peaked high-amplitude wakefields have nearly the same period as that of the train of drive bunches. This can lead to constructive interference between wakefields from successive bunches, so that a cumulative buildup in the amplitude of the

wakefield occurs after each bunch in the train. A test bunch injected one-half period behind the last drive bunch can experience a strong accelerating field. The superposition of wakefield amplitudes from a train of N drive bunches of charge q can lead to an accelerating field comparable to that produced by a single, equally dimensioned bunch of charge $Q=Nq$. But, since it is easier to produce a short, well-focused bunch of lower charge, and since shorter bunches produce stronger wakefields, considerable advantage may accrue when a train of moderate-charge short bunches is employed, rather than a single bunch of the same total charge.

The analysis presented in Ref. [1] was for the simple, albeit unattainable, two-dimensional configuration of an infinitesimally thin sheet beam passing along the axis between two parallel dielectric slabs having perfectly conducting exterior coatings. In Ref. [3], preliminary results were presented for acceleration in a cylindrical waveguide, consisting of a dielectric tube with a perfectly conducting outer coating, with the charge bunches moving along the axis. Results were shown in Ref. [3] in which an unloaded acceleration gradient of about 57 MeV/m was predicted using a single 2-nC drive bunch in a suitably designed dielectric-lined waveguide. But the theory expounded in Refs. [1] and [3] contained several flaws which will be recounted below, and which are remedied in the present work. Numerical computations presented in the present paper show, for the example cited in Ref. [3], with a single 2-nC rectangular bunch of 0.18-mm length and with waveguide inner and outer radii of 0.375 and 4.88 mm, that an accelerating gradient of 131 MeV/m can be obtained. A gradient of this magnitude, using a moderate-strength

*Permanent address: POSTECH, Pohang, Korea. Electronic address: sypark@postech.ac.kr

†Electronic address: jay.hirshfield@yale.edu

bunch charge, is in the range sought for a future TeV-class linear collider. This preliminary result suggests that careful analysis be devoted to fully understand this new approach for achievement of high-gradient electron-positron acceleration, to perfect means for generating kA, sub-psec electron bunches, and to provide the basis for design of proof-of-principal experiments. This paper concentrates mainly on formal aspects of the theory of wakefield excitation in a dielectric-lined waveguide. The theory applies to the wakefields within a drive bunch, to the wakefields behind a single drive bunch, and to the composite wakefields of a train of drive bunches. However, to avoid undue length, numerical examples are given in this paper only for a single drive bunch.

A major concern in any accelerator configuration is orbit instability driven by transverse forces that arise from nonaxisymmetric bunch distributions. That concern is addressed in this paper, in which theory is developed for excitation of hybrid electric-magnetic (HEM) modes excited by a nonaxisymmetric bunch, or train of such bunches. Theories along this line have been developed heretofore, including those by Rosing and Gai [4], and by Ng [5], but these authors did not agree with one another on some important issues. These prior theories are not based on an expansion of the wave equation in a sequence of orthonormal waveguide modes, so their treatment of multimode, multibunch effects may be more cumbersome than the normal-mode expansion method that is expounded in this paper. This follows since direct solution of the inhomogeneous coupled wave equations for the wakefields induced by a short bunch moving along a dielectric-lined waveguide without expansion in normal modes requires a summation over a large number of poles in a transform integral, with a concomitant evaluation of a large number of implicit residues. The normal-mode approach requires summation over only two poles, with explicit residues. The normal-mode theory presented here will also be shown to lead to compact formulas for the longitudinal and transverse monopole, dipole and higher-order forces on a test bunch that follows behind an off-axis drive bunch, and for the radiated power. All results given in this paper can easily be generalized to a train of drive bunches, including conditions where the wakefields interfere constructively. The chief objective of this work is to provide a systematic theory of dielectric wakefields and their application to acceleration, and to allow scrutiny of potential beam instabilities driven by off-axis excursions of the drive bunches, including the case of a synchronous multibunch train.

In working toward that objective, several previously unexplored theoretical issues had to be confronted. Although field solutions and dispersion relations for HEM modes for a cylindrical dielectric-lined waveguide were derived long ago [6], no detailed orthonormalization relation was previously obtained; this deficiency is now remedied. Furthermore, the distinction between orthonormalization, when modes are excited by a stationary source or by a moving source, were not clarified, in particular the need to modify the orthonormalization relation obtained for a stationary source when the source is a uniformly moving charge bunch; this deficiency is also now remedied. That distinction was not recognized in Refs. [1] and [3]. Calculation of the radiated power from a moving charge bunch in a dielectric waveguide is

furthermore shown to require accounting for the convected Coulomb field energy that trails a bunch. Subtracting this from the Poynting flux gives the radiated power, and thus the drag force on the bunch. The drag force found in this way agrees identically with that found from wakefields acting directly on the bunch, as of course it must. The radiated power is shown to propagate in a direction *opposite* to that of the bunch. This subtle point was also not recognized in Refs. [1] and [3], so that calculations therein of the drag force only from the accumulation of stored wakefield energy are incorrect. A recently published power flow model for wake fields in a dielectric waveguide [7] led to somewhat different conclusions from those presented here, including even the direction of power flow.

In addition to exposition of the theory as described above, numerical results are presented of monopole, dipole, and quadrupole wakefields induced by the passage of a single bunch. Plots of electric field lines for the monopole case are presented to help understand the unusual nature of the fields. Numerical results are also presented for transverse forces arising from a bunch displaced from the axis, and for the radiated power. Future papers will deal with detailed multibunch computations, including acceleration of a test bunch; detailed stability analysis for a single bunch and a train of bunches; and effects such as end reflections of wakefields that are peculiar to finite-length realistic accelerating modules.

II. WAKEFIELDS IN A DIELECTRIC-LINED CYLINDRICAL WAVEGUIDE

To introduce the notation, we review the derivation for the fields of HEM modes of a cylindrical waveguide containing one or more axisymmetric dielectric layers. A further derivation is given, evidently for the first time, for the orthonormalization relation to be used when these modes are excited by a stationary source, and when they are excited by a moving source. Field solutions are obtained when the source is a moving charge bunch, corresponding to Cerenkov radiation in a transversely bounded system. The fields obtained are shown to be consistent with Gauss's law. Forces arising from wakefields are found, including those within the bunch and those that can act upon (and accelerate) a test bunch that trails a drive bunch; these forces are found to conform to the Panofsky-Wenzel theorem [8]. Poynting's theorem is examined, and it is shown that convected Coulomb field energy needs to be subtracted from the Poynting flux to find the correct radiation power flow, and thus the radiation reaction force (or drag force) acting on a radiating bunch; the drag force is found to be consistent with Wilson's theorem [9]; the direction of radiation power flow is found to be opposite to motion of the bunch. These results are generalized to bunches of arbitrary length and charge distribution, and to a train of such bunches.

A. Eigenmodes for cylindrical waveguide with coaxial dielectric liners

In this section, the electromagnetic fields of a cylindrical waveguide containing one or more coaxial dielectric layers are determined. The fields are shown to be expressible in terms of normal modes that, in general, are hybrid modes

with six field components. However, for the special case of azimuthally symmetric modes it can be shown that the hybrid modes reduce to transverse-electric (TE) and transverse-magnetic (TM) types. The most common form for a dielectrically loaded cylindrical waveguide is that of a hollow uniform dielectric pipe with a vacuum hole along its axis, and with an ideally conducting layer on its exterior surface. The fields and dispersion relation for hybrid HEM modes of this structure have been long known [6] but, prior to the work reported here, there seems to have been no derivation of an orthogonality relationship, nor of the power-flow formula. For solution of the wave equation with source charges and currents of a bunch moving in the central vacuum hole of such a waveguide, an orthonormalization procedure is necessary to decompose the sources into normal modes.

Fourier expansion of the fields in a circular cylindrical waveguide takes the form

$$\begin{pmatrix} E_z(\mathbf{r}, t) \\ E_r(\mathbf{r}, t) \\ E_\theta(\mathbf{r}, t) \\ H_z(\mathbf{r}, t) \\ H_r(\mathbf{r}, t) \\ H_\theta(\mathbf{r}, t) \end{pmatrix} = \frac{1}{(2\pi)^3} \int_{-\infty}^{\infty} d\omega dk \times \sum_{l=-\infty}^{\infty} \exp[-i(\omega t - kz - l\theta)] \times \begin{pmatrix} e_z(r) \\ i e_r(r) \\ -e_\theta(r) \\ -i h_z(r) \\ h_r(r) \\ i h_\theta(r) \end{pmatrix}. \quad (2.1)$$

Then $e_z(r)$ and $h_z(r)$ satisfy Bessel's equation

$$\left[\frac{d^2}{dr^2} + \frac{1}{r} \frac{d}{dr} + \left(k_\perp^2 - \frac{l^2}{r^2} \right) \right] \begin{pmatrix} e_z(r) \\ h_z(r) \end{pmatrix} = 0, \quad (2.2)$$

where $k_\perp^2 \equiv \varepsilon \mu (\omega/c)^2 - k^2$, and where the transverse components are given by

$$\begin{pmatrix} e_r(r) \\ h_\theta(r) \end{pmatrix} = \frac{1}{k_\perp^2} \left[\begin{pmatrix} k \\ \varepsilon \frac{\omega}{c} \end{pmatrix} \frac{de_z}{dr} + \begin{pmatrix} \mu \frac{\omega}{c} \\ k \end{pmatrix} \frac{l}{r} h_z \right]$$

and

$$\begin{pmatrix} h_r(r) \\ e_\theta(r) \end{pmatrix} = \frac{1}{k_\perp^2} \left[\begin{pmatrix} k \\ \mu \frac{\omega}{c} \end{pmatrix} \frac{dh_z}{dr} + \begin{pmatrix} \varepsilon \frac{\omega}{c} \\ k \end{pmatrix} \frac{l}{r} e_z \right]. \quad (2.3)$$

In the vacuum hole ($0 < r < R_1$) where $\varepsilon = \mu = 1$, the fields must be regular at $r = 0$; thus

$$\begin{pmatrix} e_z(r) \\ h_z(r) \end{pmatrix} = \begin{pmatrix} A \\ B \end{pmatrix} \frac{I_l(x)}{I_l(x_1)}, \quad (2.4)$$

where $I_l(x)$ is the modified Bessel function, and

$$x \equiv |k_\perp^{(1)}| r, \quad x_1 \equiv |k_\perp^{(1)}| R_1, \quad \text{and} \quad (k_\perp^{(1)})^2 \equiv (\omega/c)^2 - k^2 < 0.$$

To find fields in the dielectric region ($R_1 < r < R_2$) where $\varepsilon = \varepsilon_2$ and $\mu = \mu_2$, appropriate boundary conditions must be satisfied. At the outer conducting boundary one has $e_z(R_2) = e_\theta(R_2) = h_r(R_2) = 0$, these being equivalent to simply $e_z(R_2) = dh_z(R_2)/dr = 0$. Thus

$$\begin{pmatrix} e_z(r) \\ h_z(r) \end{pmatrix} = \begin{pmatrix} A \frac{E_l(y)}{E_l(y_1)} \\ B \frac{H_l(y)}{H_l(y_1)} \end{pmatrix}, \quad (2.5)$$

where

$$\begin{pmatrix} E_l(y) \\ H_l(y) \end{pmatrix} \equiv J_l(y) \begin{pmatrix} N_l(y_2) \\ N'_l(y_2) \end{pmatrix} - N_l(y) \begin{pmatrix} J_l(y_2) \\ J'_l(y_2) \end{pmatrix} \quad (2.6)$$

with $y \equiv k_\perp^{(2)} r$, $y_1 \equiv k_\perp^{(2)} R_1$, $y_2 \equiv k_\perp^{(2)} R_2$, and $(k_\perp^{(2)})^2 \equiv \varepsilon \mu (\omega/c)^2 - k^2 > 0$, which choice of sign is required for nonevanescant radiation. In Eq. (2.6), $J_l(y)$ and $N_l(y)$ are ordinary Bessel functions of the first and second kinds.

The remaining boundary conditions are that e_z , h_z , e_θ , and h_θ be continuous at $r = R_1$. With these boundary conditions, Eqs. (2.3)–(2.6) can be combined to find the unknown coefficients A and B , with the result given in matrix form as

$$\begin{pmatrix} M_{11} M_{12} \\ M_{21} M_{22} \end{pmatrix} \begin{pmatrix} A \\ B \end{pmatrix} = 0, \quad (2.7a)$$

where

$$\begin{aligned} M_{11} &= \frac{I'_l(x_1)}{x_1 I_l(x_1)} + \varepsilon \frac{E'_l(y_1)}{y_1 E_l(y_1)}, \\ M_{22} &= \frac{I'_l(x_1)}{x_1 I_l(x_1)} + \mu \frac{H'_l(y_1)}{y_1 H_l(y_1)}, \\ M_{12} = M_{21} &= \frac{kcl}{\omega} \left(\frac{1}{x_1^2} + \frac{1}{y_1^2} \right), \end{aligned} \quad (2.7b)$$

with the primed functions representing a derivative with respect to the argument. Equation (2.7a) gives the dispersion relation as

$$\det M = M_{11} M_{22} - M_{12}^2 = 0, \quad (2.8a)$$

and the TE/TM mixing ratio as

$$\frac{B}{A} = - \frac{M_{12}}{M_{11}}. \quad (2.8b)$$

The remaining boundary conditions, namely, that εe_r and μh_r be continuous at $r = R_1$, do not give additional independent conditions, because $\varepsilon (\omega/c) e_r = (l/r) e_z + k h_\theta$ and $\mu (\omega/c) h_r = (l/r) h_z + k e_\theta$.

The dispersion relation [Eq. (2.8a)] can be satisfied by a discrete set of eigenvalues with $k_{\perp n}^2 = -k_n^2 + \varepsilon \mu \omega_n^2/c^2$; the corresponding eigenfunctions will be designated by subscripts such as $e_{z,n}(r)$, $h_{z,n}(r)$, etc.

B. Generalized orthonormality relations

In Appendix A it is proven that, for N concentric dielectric layers in a uniform cylindrical waveguide, the following generalized orthogonality relation applies between any two modes satisfying the dispersion relation with frequencies and wave numbers (ω_m, k_m) and (ω_n, k_n) ,

$$\sum_{i=1}^N [(k_{\perp,m}^{(i)})^2 - (k_{\perp,n}^{(i)})^2] \int_{R_{i-1}}^{R_i} dr r [e_{r,m}(r)h_{\theta,n}(r) + e_{\theta,m}(r)h_{r,n}(r)] = 0, \quad \text{if } m \neq n, \quad (2.9)$$

where $k_{\perp,n}^{(i)} = \sqrt{\varepsilon_i \mu_i (\omega_n/c)^2 - k_n^2}$ is the radial eigenvalue for the transverse wave number for the n th mode in the i th dielectric layer. As in Sec. II A, the specific configuration of interest in this paper is that of a vacuum hole ($i=1$; $0 < r < R_1$) surrounded by a single dielectric layer ($i=2$; $R_1 < r < R_2$), but generalization of the orthonormality relation to an arbitrary number of layers will be maintained throughout this section. As will be shown below, the means of applying Eq. (2.9) to find the normalization constant when $m=n$ will depend upon the nature of the source of radiation.

For a waveguide with stationary sources, solutions of Maxwell's equations are symmetric in time, so that all waveguide modes can be taken to have equal frequencies, i.e., $\omega_m = \omega_n$. Thus $(k_{\perp,m}^{(i)})^2 - (k_{\perp,n}^{(i)})^2 = -(k_m^2 - k_n^2)$ is independent of the layer parameters, and moves outside of the summation in Eq. (2.9). The following orthonormality relation then results:

$$\sum_{i=1}^N \int_{R_{i-1}}^{R_i} dr r [e_{r,m}(r)h_{\theta,n}(r) + e_{\theta,m}(r)h_{r,n}(r)] = \delta_{mn} C'_n, \quad (2.10)$$

where C'_n is the normalization constant to be used with stationary sources. A general relation for orthogonality similar to this has been derived in Ref. [10], although the proof there was limited to waveguides containing only singly connected domains of different dielectric constants; the proof provided here applies to multiply connected domains typified by a coaxial structure of several axisymmetric layers of different dielectric constant. The explicit form of C'_n is given in Eq. (A14).

However, when sources of radiation within the waveguide are charge bunches moving parallel to, or along, the axis with velocity v , the correct symmetry is with respect to $z - vt$, so that $\omega_m = k_m v$. Now $(k_{\perp,m}^{(i)})^2 - (k_{\perp,n}^{(i)})^2 = (\varepsilon_i \mu_i \beta^2 - 1)(k_m^2 - k_n^2)$, where $\beta = v/c$, so from Eq. (2.9) one obtains the modified orthonormality relation

$$\sum_{i=1}^N (\varepsilon_i \mu_i \beta^2 - 1) \int_{R_{i-1}}^{R_i} dr r [e_{r,m}(r)h_{\theta,n}(r) + e_{\theta,m}(r)h_{r,n}(r)] = \delta_{mn} \beta C_n, \quad (2.11)$$

where C_n is the normalization constant to be used when a uniformly moving charge bunch is the source of the fields, and where the factor β on the right-hand side is introduced to simplify the form of C_n (see below). The factor $(\varepsilon_i \mu_i \beta^2 - 1)$ was introduced in Ref. [1] as an *ad hoc* weighting fac-

tor in the Green's function for wakefields in a two-dimensional waveguide; its precise origin is identified here. Carrying out the integration in Eq. (2.11) (see Appendix A) gives the following result for the normalization constant in terms of the eigenfunctions $e_{z,n}(r)$ and $h_{z,n}(r)$:

$$C_n = \sum_{i=1}^N \frac{r^2}{2} \left\{ \varepsilon_i \left[\frac{1}{k_{\perp,n}^2} \left(\frac{de_{z,n}}{dr} \right)^2 + \left(1 - \frac{l^2}{k_{\perp,n}^2 r^2} \right) e_{z,n}^2 \right] + \mu_i \left[\frac{1}{k_{\perp,n}^2} \left(\frac{dh_{z,n}}{dr} \right)^2 + \left(1 - \frac{l^2}{k_{\perp,n}^2 r^2} \right) h_{z,n}^2 \right] \right\} \Bigg|_{R_{i-1}}^{R_i}. \quad (2.12)$$

As further shown in Appendix A, from Eq. (2.11) it is possible to derive another, simpler form of the orthonormality relation, namely,

$$\sum_{i=1}^N \int_{R_{i-1}}^{R_i} dr r [\varepsilon_i e_{z,m}(r)e_{z,n}(r) + \mu_i h_{z,m}(r)h_{z,n}(r)] = C_n \delta_{mn}, \quad (2.13)$$

with C_n as in Eq. (2.12). This latter form will be used to solve the wave equation with a moving source for wakefields in Sec II C while the form given by Eq. (2.11) will be used in a calculation of the radiation power in Sec. II F.

C. Wave equations with moving charge bunch as a Source

We consider as a source for the wakefields a point charge (or a short rigid bunch) of charge q_0 moving with a constant velocity v in a dielectric-lined cylindrical waveguide of the type discussed in Sec. II A. Its direction of motion is along the z axis, but its transverse position is displaced off the axis by an increment r_0 in the direction chosen to be $\theta_0 = 0$, i.e., along the x -axis. Thus for the point charge one has

$$\rho(\mathbf{r}, t) = q_0 \frac{\delta(r - r_0)}{r} \delta(\theta) \delta(s), \quad (2.14)$$

$$J_z(\mathbf{r}, t) = v \rho(\mathbf{r}, t), \quad J_r = J_\theta = 0,$$

where $s \equiv z - vt$. As will be shown below, the field solution for a distributed source can be found by replacing the δ function $\delta(s)$ in Eq. (2.14) by the distribution function $f(s)$, where $\int ds f(s) = 1$; now the solution can be constructed from that for a δ -function source by observing that

$$f(s) = \int_{-\infty}^{\infty} ds' f(s') \delta(s - s'), \quad (2.15)$$

and that the solutions of Maxwell's equations are linear in the source terms. Therefore, the solution for a δ -function source will be found first, and its extension to a distributed source will then follow easily using the prescription of Eq. (2.15).

One can expand the fields as in Eqs. (2.1), and substitute these into Maxwell's field equations, with the source terms given by Eq. (2.14). The longitudinal components of the fields are found to satisfy Bessel's equation with a source term on the right-hand side, e.g.,

$$\left[\frac{d^2}{dr^2} + \frac{1}{2} \frac{d}{dr} + \left(k_{\perp}^2 - \frac{l^2}{r^2} \right) \right] \begin{pmatrix} e_z(r) \\ h_z(r) \end{pmatrix} = \begin{pmatrix} \tilde{J}_z(r) \\ 0 \end{pmatrix}, \quad (2.16)$$

where $k_{\perp}^2 \equiv \varepsilon \mu \omega^2 / c^2 - k^2$, and

$$\begin{aligned} \tilde{J}_z(r) &= 4\pi \int_{-\infty}^{\infty} dt \int_{-\infty}^{\infty} dz \int_0^{2\pi} d\theta e^{i(\omega t - kz - l\theta)} \\ &\times \left[\frac{1}{\varepsilon} \frac{\partial \rho}{\partial z} + \frac{\mu}{c^2} \frac{\partial J_z}{\partial t} \right] \\ &= 8\pi^2 i q_0 k (1 - \beta^2) \frac{\delta(r - r_0)}{r} \delta(\omega - kv), \end{aligned} \quad (2.17)$$

since $\varepsilon = \mu = 1$ in the vacuum channel. The transverse field components are given by Eqs. (2.3), since $J_r = J_{\theta} = 0$.

We now proceed to solve Eq. (2.16) by expanding the fields $e_z(r)$ and $h_z(r)$ in terms of their eigenmodes, as

$$\begin{pmatrix} e_z(r) \\ h_z(r) \end{pmatrix} = \sum_{n=1}^{\infty} A_n \begin{pmatrix} e_{z,n}(r) \\ h_{z,n}(r) \end{pmatrix}. \quad (2.18)$$

Upon substituting Eq. (2.18) into Eq. (2.16) and noting that the eigenmodes $e_{z,n}(r)$ and $h_{z,n}(r)$ satisfy the source-free relation [Eq. 2.2] with eigenvalue $k_{\perp,n}$, one obtains

$$\sum_{n=1}^{\infty} A_n (k_{\perp}^2 - k_{\perp,n}^2) \begin{pmatrix} e_{z,n}(r) \\ h_{z,n}(r) \end{pmatrix} = \begin{pmatrix} \tilde{J}_z(r) \\ 0 \end{pmatrix}. \quad (2.19)$$

Now the orthonormality relation [Eq. (2.13)] can be used to find the amplitudes A_n , namely

$$A_n(k) = \frac{\tilde{W}_n(k)}{k^2 - k_n^2}, \quad (2.20)$$

where

$$\begin{aligned} \tilde{W}_n(k) &\equiv \frac{1}{C_n} \sum_{i=1}^N \frac{1}{\varepsilon_i \mu_i \beta^2 - 1} \int_{R_{i-1}}^{R_i} dr r e_{z,n}(r) \tilde{J}_z(r) \\ &= -\frac{8\pi^2 i}{C_n} q_0 e_{z,n}(r_0) k \delta(\omega - kv). \end{aligned} \quad (2.21)$$

Substituting $A_n(k)$ into Eq. (2.18), using Eqs. (2.1) and (2.3), yields the following solution for the fields:

$$\begin{pmatrix} E_z(r,t) \\ E_r(r,t) \\ H_{\theta}(r,t) \\ H_z(r,t) \\ H_r(r,t) \\ E_{\theta}(r,t) \end{pmatrix} = \frac{q_0}{i\pi} \sum_{l=-\infty}^{\infty} e^{il\theta} \sum_{n=1}^{\infty} \frac{e_{z,n}(r_0)}{C_n} \int_{-\infty}^{\infty} dk \frac{ke^{iks}}{k^2 - k_n^2} \times \begin{pmatrix} e_{z,n}(r) \\ \frac{k}{k_{\perp}^2} \frac{k_{\perp,n}^2}{k_n} \begin{pmatrix} i e_{r,n}(r) \\ -h_{\theta,n}(r) \end{pmatrix} \\ i h_{z,n}(r) \\ \frac{k}{k_{\perp}^2} \frac{k_{\perp,n}^2}{k_n} \begin{pmatrix} h_{r,n}(r) \\ i e_{\theta,n}(r) \end{pmatrix} \end{pmatrix}. \quad (2.22)$$

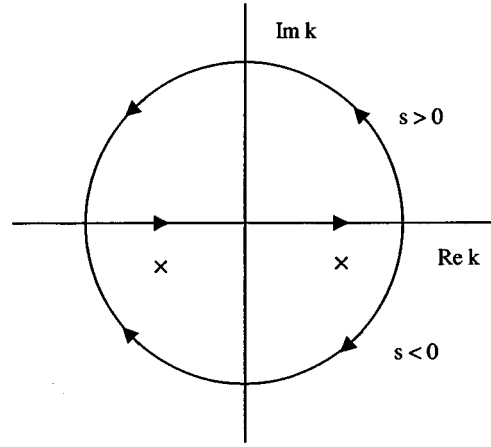


FIG. 1. Contours for integration in the complex k plane for wakefields. Note that both poles are in the lower-half plane to be consistent with causality. The upper contour ($s > 0$) corresponds to the region ahead of the beam, while the lower contour ($s < 0$) corresponds to the region behind the beam.

In order to carry out the k integration in Eq. (2.22), one needs a prescription for handling the singularities in the integrand at $k = \pm k_n$; this prescription is supplied by the requirement of causality. For the wakefield problem, the proper causality condition is that there be no fields ahead of a source charge. This condition can be met by shifting both poles into the lower half of the (complex) k plane, as shown in Fig. 1. The k integration is then carried out along the contours shown in Fig. 1, closing in the upper-half-plane for $s > 0$, and closing in the lower-half plane for $s < 0$. The contour chosen for evaluation of a similar integral in Ref. [1] only enclosed one pole in the lower-half k plane, and thus provided only half of the correct result. Evaluation of the k integrals in Eq. (2.22) thus gives

$$\begin{aligned} &\int_{-\infty}^{\infty} dk \frac{e^{iks}}{k^2 - k_n^2} \begin{pmatrix} k \\ k^2/k_{\perp}^2 \end{pmatrix} \\ &= -2\pi i \begin{pmatrix} \cos k_n s \\ (i k_n / k_{\perp,n}^2) \sin k_n s \end{pmatrix} \Theta(-s), \end{aligned} \quad (2.23)$$

where

$$\Theta(x) = \begin{cases} 1 & \text{if } x > 0 \\ 0 & \text{if } x < 0 \end{cases}$$

is the Heaviside function. Substituting Eq. (2.23) into Eq. (2.22), and taking real parts, gives the field solutions as follows:

$$\begin{pmatrix} E_z(\mathbf{r},t) \\ E_r(\mathbf{r},t) \\ H_\theta(\mathbf{r},t) \\ H_z(\mathbf{r},t) \\ H_r(\mathbf{r},t) \\ E_\theta(\mathbf{r},t) \end{pmatrix} = -2q_0 \sum_{l=-\infty}^{\infty} \sum_{n=1}^{\infty} \frac{e_{z,n}(r_0)}{C_n} \times \begin{pmatrix} e_{z,n}(r)g_{z,n}^0(s)\cos l\theta \\ \begin{pmatrix} -e_{r,n}(r) \\ -h_{\theta,n}(r) \end{pmatrix} g_{\perp,n}^0(s)\cos l\theta \\ h_{z,n}(r)g_{z,n}^0(s)\sin l\theta \\ \begin{pmatrix} -h_{r,n}(r) \\ e_{\theta,n}(r) \end{pmatrix} g_{\perp,n}^0(s)\sin l\theta \end{pmatrix}, \quad (2.24)$$

where

$$\begin{pmatrix} g_{z,n}^0(s) \\ g_{\perp,n}^0(s) \end{pmatrix} \equiv \begin{pmatrix} \cos k_n s \\ \sin k_n s \end{pmatrix} \Theta(-s).$$

Since $e_{z,n}(r)$, $e_{r,n}(r)$, and $h_{\theta,n}(r)$ are even functions of l , and since $h_{z,n}(r)$, $h_{r,n}(r)$, and $e_{\theta,n}(r)$ are odd functions of l , the terms under the summation in Eq. (2.24) are all even functions of l . Thus the summation may be condensed to run from 0 to ∞ , doubling the value of all the terms except that for $l=0$.

For a distributed source, as given by Eq. (2.15), the fields are still given by equations of the same form as Eq. (2.24), but the following generalization of the g functions is used:

$$\begin{pmatrix} g_{z,n}^0(s) \\ g_{\perp,n}^0(s) \end{pmatrix} \rightarrow \begin{pmatrix} g_{z,n}(s) \\ g_{\perp,n}(s) \end{pmatrix} = \int_{-\infty}^{\infty} ds' f(s') \begin{pmatrix} g_{z,n}^0(s-s') \\ g_{\perp,n}^0(s-s') \end{pmatrix}. \quad (2.25)$$

For a train of M distributed bunches, the distribution function can be represented as

$$f(s) = \sum_{j=1}^M f_j(s-s_j), \quad (2.26)$$

where $s_j = z - z_j - v_j t$, with z_j the centroid for the j th bunch and v_j its velocity. This prescription may be employed in analysis of the wakefields for a train of bunches, but detailed discussion of multibunch wakes is beyond the scope of this paper.

D. Electric flux and Gauss's law

A check on the accuracy of the overall field solution given by Eq. (2.24) can be obtained by calculating the total electric flux that emanates from the charge bunch using Gauss's law. This check can be carried out easily in two limiting cases: (i) numerically in the limit as $\gamma \rightarrow \infty$, and (ii) analytically in the limit as $R_1 \rightarrow 0$.

Only the monopole field components ($l=0$) contribute to the total flux, after integration over θ . Thus the electric field components that contribute to the flux are

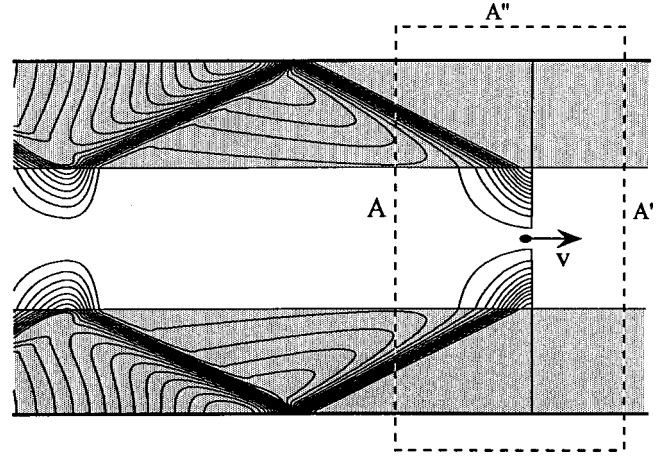


FIG. 2. Gaussian pillbox used to calculate the electric flux and power flow emerging out of the beam. Here, and in Figs. 5 and 6, the bunch is at the right-hand end of the plot and is moving toward the right. For checking consistency with Gauss's law, surface A is positioned immediately behind the charge, while for calculating power flow, surface A is positioned at an arbitrary distance behind the charge. The pillbox is fixed in space, while the beam is moving.

$$\begin{pmatrix} E_z(\mathbf{r},t) \\ E_r(\mathbf{r},t) \end{pmatrix}_{l=0} = -\frac{4q_0}{R_1^2} \sum_{n=1}^{\infty} \frac{e_{z,n}(r_0)}{\bar{C}_n} \times \begin{pmatrix} e_{z,n}(r)g_{z,n}^0(s) \\ -\frac{k_n}{k_{\perp,n}^2} \frac{de_{z,n}(r)}{dr} g_{\perp,n}^0(s) \end{pmatrix}, \quad (2.27)$$

where

$$\bar{C}_n \equiv \left(\frac{2}{R_1^2} \right) C_n = \sum_{i=1}^2 \left(\frac{r}{R_1} \right)^{2i} \left[\frac{1}{k_{\perp,n}^2} \left(\frac{de_{z,n}}{dr} \right)^2 + e_{z,n}^2 \right]_{R_{i-1}}^{R_i}. \quad (2.28)$$

For the monopole case, the only magnetic field component is $H_\theta(\mathbf{r},t) = \epsilon\beta E_r(\mathbf{r},t)$.

We now consider a Gaussian pillbox, as shown in Fig. 2, and calculate the total electric flux emanating from it. The only nonvanishing contribution comes from field lines that pass across surface A . If the location of surface A is taken to be just behind the charge bunch (i.e., in the limit as $s \rightarrow 0^-$) the preponderance of the contribution to the flux comes in the vacuum channel. Furthermore, in the limit as $\gamma \rightarrow \infty$, $|k_{\perp,n}^{(1)}| = k_n/\gamma \rightarrow 0$, and thus the field becomes uniform in radius, i.e., $e_{z,n}(r) = I_0(|k_{\perp,n}^{(1)}|r) \rightarrow 1$, and similarly $e_{z,n}(r_0) \rightarrow 1$. Therefore the total flux of electric field Φ emanating from the pillbox becomes

$$\Phi \rightarrow \pi R_1^2 [-E_z(s \rightarrow 0^-)] = 4\pi q_0 \sum_{n=1}^{\infty} \frac{1}{\bar{C}_n}. \quad (2.29)$$

It can be demonstrated by numerical evaluation that the sum in Eq. (2.29) approaches unity, as it must be consistent with Gauss's law.

Analytically, a proof of consistency with Gauss's law can be obtained in the limit as $R_1 \rightarrow 0$. In this limit, the dispersion relation for TM_{0n} modes of the dielectric-filled waveguide [Eq. (2.8)] reduces to

$$J_0(k_{\perp,n}^{(2)} R_2) = 0, \quad (2.30)$$

and thus $k_{\perp,n}^{(2)} = j_{0n}/R_2$, where $J_0(j_{0n}) = 0$. The electric field components in the waveguide are now

$$\begin{pmatrix} E_z(r,t) \\ E_r(r,t) \end{pmatrix} = -\frac{4q_0}{\epsilon R_2^2} \sum_{n=1}^{\infty} \frac{1}{J_1^2(j_{0n})} \begin{pmatrix} J_0(y) g_{z,n}^0(s) \\ \frac{J_1(y)}{\sqrt{\epsilon \mu \beta^2 - 1}} g_{\perp,n}^0(s) \end{pmatrix}, \quad (2.31)$$

where $y \equiv k_{\perp,n}^{(2)} r$. We consider the same pillbox as shown in Fig. 2, and go to the limit as $s \rightarrow 0^-$. To carry out the proof, we employ the following (relatively obscure) identity, which can be proven from the general properties of orthogonal eigenfunctions; this identity was previously employed in Ref. [13].

$$\sum_{n=1}^{\infty} \frac{J_0\left(\frac{r}{R_2} j_{0n}\right)}{J_1^2(j_{0n})} = \frac{R_2^2}{2} \frac{\delta(r)}{r}. \quad (2.32)$$

Use of Eq. (2.32) allows a computation of the flux, yielding the result

$$\Phi = 2\pi \int_{R_1 \rightarrow 0}^{R_2} dr r [-E_z(r)]_{s \rightarrow 0^-} = 4\pi \frac{q_0}{\epsilon}, \quad (2.33)$$

again consistent with Gauss's law.

Both of the demonstrations given in this section show that the results obtained in this paper for the wakefields of a charge bunch are consistent with Gauss's law, at least in the limits taken. Presumably, a general proof can be obtained, but such a proof is beyond the scope of this paper.

E. Forces arising from wakefields

A test charge q that follows a drive bunch of charge q_0 will experience a Lorentz force \mathbf{F} , with components given by

$$\begin{pmatrix} F_z \\ F_r \\ F_\theta \end{pmatrix} = q \begin{pmatrix} E_z \\ E_r - \mu \beta H_\theta \\ E_\theta + \mu \beta H_r \end{pmatrix}. \quad (2.34)$$

Substituting the fields as given by Eq. (2.24) into this equation, and performing algebraic manipulations using Eq. (2.3), enables one to derive the following remarkably simple form for the components of \mathbf{F} :

$$\begin{pmatrix} F_z(\mathbf{r}, t) \\ F_r(\mathbf{r}, t) \\ F_\theta(\mathbf{r}, t) \end{pmatrix} = -2q q_0 \sum_{l=-\infty}^{\infty} \sum_{n=1}^{\infty} \frac{e_{z,n}(r_0)}{C_n} \times \begin{pmatrix} e_{z,n}(r) g_{z,n}^0(s) \cos l\theta \\ \frac{1}{k_n} \frac{de_{z,n}}{dr} g_{\perp,n}^0(s) \cos l\theta \\ -\frac{1}{k_n} \frac{l}{r} e_{z,n}(r) g_{\perp,n}^0(s) \sin l\theta \end{pmatrix}. \quad (2.35)$$

It is important to point out that Eq. (2.35) satisfies the Panofsky-Wenzel theorem [8], in that it is consistent with the relation

$$\nabla_{\perp} F_z = \frac{\partial}{\partial z} \mathbf{F}_{\perp}. \quad (2.36)$$

Furthermore, one can immediately verify that the force given by Eq. (2.35) can be written as the gradient of a scalar function φ , namely,

$$\mathbf{F} = -q \nabla \varphi, \quad (2.37)$$

where φ may be thought of as a pseudopotential defined by

$$\varphi(\mathbf{r}, t) = 2q_0 \sum_{l=-\infty}^{\infty} \sum_{n=1}^{\infty} \frac{e_{z,n}(r_0) e_{z,n}(r)}{k_n C_n} g_{\perp,n}^0(s) \cos l\theta. \quad (2.38)$$

This form can prove useful in exploring stability of the beam.

The drag force on a drive bunch can be calculated by considering the bunch to have a finite length of uniform line charge density, calculating the forces acting on each part of the bunch using Eq. (2.35), and then taking the limit as the bunch length goes to zero. Since the wakefields can exert a force only on those charge elements behind it, one obtains the drag force as

$$F_{z,\text{drag}} = \frac{1}{2} F_z(\mathbf{r}, t) \Big|_{\substack{r \rightarrow r_0 \\ \theta \rightarrow 0 \\ s \rightarrow 0^-}} = -q_0^2 \sum_{l=-\infty}^{\infty} \sum_{n=1}^{\infty} \frac{e_{z,n}^2(r_0)}{C_n}. \quad (2.39)$$

The transverse components of the force of a point charge bunch upon itself vanish since $g_{\perp,n}^0(s=0) = 0$. The factor of $\frac{1}{2}$ appearing in Eq. (2.39) is often referred to as arising from the *fundamental theorem of beam loading*, or Wilson's theorem [9]. This theorem can be proven for a general distribution of charge in the bunch, as long as the bunch is narrow in s . This follows from a consideration of the integral:

$$\begin{aligned} & \int_{-\infty}^{\infty} ds f(s) \int_{-\infty}^{\infty} ds_0 f(s_0) g_{z,n}^0(s-s_0) \Big|_{s,s_0 \rightarrow 0^-} \\ &= \int_{-\infty}^{\infty} ds f(s) \int_{-\infty}^{\infty} ds_0 f(s_0) \Theta(s_0 - s) = \frac{1}{2}. \end{aligned} \quad (2.40)$$

The force terms given by Eq. (2.35) exhibit useful scaling forms in the limit as $\gamma \rightarrow \infty$. Both the drive charge q_0 and the test charge q are moving in the vacuum channel $r < R_1$ where $e_{z,n}(r) = I_l(x)/I_l(x_1) \rightarrow (r/R_1)^l$, where $x \equiv |k_{\perp,n}^{(1)}|r$. As $\gamma \rightarrow \infty$, $x \rightarrow k_n r / \gamma \rightarrow 0$, so that the components of the force can be written

$$\begin{pmatrix} F_z(\mathbf{r}, t) \\ F_r(\mathbf{r}, t) \\ F_\theta(\mathbf{r}, t) \end{pmatrix} = -2qq_0 \sum_{l=-\infty}^{\infty} \sum_{n=1}^{\infty} \frac{1}{C_n} \left(\frac{r_0}{R_1} \right)^l \times \begin{pmatrix} \left(\frac{r}{R_1} \right)^l \cos l\theta g_{z,n}^0(s) \\ l \left(\frac{r}{R_1} \right)^{l-1} \cos l\theta g_{\perp,n}^0(s) \\ -l \left(\frac{r}{R_1} \right)^{l-1} \sin l\theta g_{\perp,n}^0(s) \end{pmatrix}. \quad (2.41)$$

Close examination of Eq. (2.41) reveals that the forces enjoy no inverse- γ scaling that might provide a qualitative advantage in stability, as compared with that for a conventional rf linac structure.

The monopole ($l=0$) and dipole ($l=\pm 1$) components are of greatest interest in determining stability. The only significant monopole component is

$$F_z|_{l=0} = -2qq_0 \sum_{n=1}^{\infty} \frac{1}{C_n} \cos k_n s \Theta(-s), \quad (2.42)$$

which is independent of γ , r_0 , and r . The monopole radial force $F_r|_{l=0}$ is zero to order γ^{-1} ; the lowest order contribution is of order γ^{-2} , as a result of the near cancellation between electric and magnetic forces. The monopole azimuthal force $F_\theta|_{l=0}$ is identically zero to all orders, by symmetry.

The dipole force is the most serious deflecting force that arises from slight displacements of the bunch off axis, on account of the $(r_0/R_1)^l$ factor in Eq. (2.41). Knowledge of the dipole force is essential in analyzing the stability of both the drive bunch or bunches, and the test bunch. The longitudinal component of the dipole force is given by

$$F_z(x, y, s)|_{l=1} = -4qq_0 \frac{r_0}{R_1} \frac{x}{R_1} \sum_{n=1}^{\infty} \frac{1}{C_n} \cos k_n s \Theta(-s), \quad (2.43)$$

since the displacement r_0 is taken to be in the x direction. (The coordinates x and y are not to be confused with the arguments x and y introduced after Eq. (2.4) in connection with the dispersion relation.) A factor of 2 in Eq. (2.43) comes from summing contributions from the $l = \pm 1$ terms. The dipole portion of the axial force is seen to be either decelerating or accelerating, depending upon the sign of x . Such an effect can contribute to energy spread within the bunch. The transverse components of the dipole force are given by

$$F_x(x, y, s)|_{l=1} = -4qq_0 \frac{r_0}{R_1} \sum_{n=1}^{\infty} \frac{1}{C_n} \frac{\sin k_n s}{k_n R_1} \Theta(-s),$$

and $F_y(x, y, s)|_{l=1} = 0. \quad (2.44)$

One notes that the transverse dipole force is proportional to r_0 , the displacement of the drive bunch off axis. Furthermore, the dipole force is zero in the direction normal to the direction of the displacement; it is independent of the position of the test charge, and is independent of γ .

F. Radiative power flow

Power radiated from a charge bunch moving along the waveguide leads to a loss of bunch energy, and is equivalent to application of an effective ‘‘drag force’’ on the bunch. This drag force can also be computed directly from the wakefields within the bunch, as is shown in Sec. II E. In this section energy loss due to radiation power flow is calculated, and the drag force derived from it is shown to equal that found in Eq. (2.39). When a train of bunches moves along the waveguide, this drag force acts in addition to forces from the wakefields from preceding bunches. Furthermore, the radiation generated by the bunch can, in principle, be coupled out of the waveguide and used, for example, as a source of radiation for spectroscopy, or for beam diagnostics, since knowledge of the spectrum of radiated power can be used to infer the bunch size. For all these reasons it is necessary to develop a theory for the radiative power flow, i.e., for the power that propagates away from the immediate vicinity of the moving bunch. As will be shown, this quantity cannot be computed from knowledge of the Poynting vector alone.

For a stationary source, radiation power flow passing through any cross section at a point along a waveguide can be calculated using the Poynting vector S_z , e.g.,

$$P_z = \int_0^{2\pi} d\theta \sum_{i=1}^N \int_{R_{i-1}}^{R_i} dr r S_z, \quad (2.45)$$

with

$$S_z = \frac{c}{4\pi} (E_r H_\theta - E_\theta H_r).$$

But for the case of a wakefield generated by a discrete bunch or bunches moving along the waveguide, we claim that not all the power flow embodied in Eq. (2.45) is a radiation power flow. This can be appreciated by considering four problems that attach to Eq. (2.45), should one interpret it as radiation power flow. (i) P_z , as calculated from Eq. (2.45), is not a uniform function of z , but exhibits sharp s -dependent peaks and valleys, as shown in computed results given in Sec. III (Fig. 8). The customary procedure of time averaging over a period of the radiation, as applied for a stationary source, cannot be applied here because the inherent symmetry with respect to $s = z - vt$ does not have a natural time period. Moreover, since the dielectric-lined waveguide structure and the drag force on the bunch are uniform along z , it is difficult to understand a radiation flow that is not also uniform in s . (ii) P_z , as calculated from Eq. (2.45), using Eq. (2.24) for the fields, cannot be written as a series of

terms that are decoupled eigenmode by eigenmode: cross terms will enter. The physical nature of these cross terms is difficult to understand. (iii) P_z , as calculated from Eq. (2.45), is not equal to the work done by the drag force on the bunch, as given by Eq. (2.39). (iv) P_z , as calculated from Eq. (2.45), is a positive quantity: the radiation would flow in the same direction as the bunch. But since the fields cannot overtake the bunch, this supposed radiation never “gets away.”

The origin of these problems can be traced to the nature of the wakefield source, which is manifestly convective, rather than stationary. As a drive bunch moves along, the Coulomb field attached to it also moves along; the Poynting flux associated with this Coulomb field appears as a power flow in Eq. (2.45) when in fact it is not radiation at all. This convected Coulomb field energy must be subtracted from P_z in order to find the true radiation power flow.

To compute true radiation power flow, we invoke the Poynting theorem as applied to a fixed volume V that at the moment of scrutiny surrounds the moving charge bunch, as depicted in Fig. 2:

$$\int_V dV \left(\frac{\partial U}{\partial t} + \nabla \cdot \mathbf{S} \right) = \int_V dV (-\mathbf{J} \cdot \mathbf{E}) = W, \quad (2.46)$$

where $U = (1/8\pi)(\epsilon \mathbf{E} \cdot \mathbf{E} + \mu \mathbf{H} \cdot \mathbf{H})$ is the electromagnetic energy density, $\mathbf{S} = (c/4\pi)\mathbf{E} \times \mathbf{H}$ is the Poynting vector, \mathbf{J} is the current density, and W is the work done by charge within the volume V . What is significant in the wakefield problem is that U and S are functions of $s = z - vt$, so that one can write Eq. (2.46) in the form

$$\begin{aligned} & \int_V dV \left[\frac{\partial}{\partial z} (S_z - vU) + \nabla_{\perp} \cdot \mathbf{S}_{\perp} \right] \\ &= \int_{A+A'} dA_z (S_z - vU) + \int_{A''} dA_{\perp} \cdot \mathbf{S}_{\perp} = W. \end{aligned} \quad (2.47)$$

If one chooses the area A'' to be just outside the perfectly conducting outer waveguide wall, and chooses A' to be in front of the bunch, fields are zero on these areas, and Eq. (2.47) reduces to an energy balance equation

$$\int_A dA_z (S_z - vU) = W. \quad (2.48)$$

Thus, in the case of wakefields, a modified Poynting vector $\bar{S}_z \equiv S_z - vU$ emerges naturally for calculating the true radiation power flow \bar{P}_z , according to

$$\bar{P}_z \equiv \int_0^{2\pi} d\theta \sum_{i=1}^N \int_{R_{i-1}}^{R_i} dr r \bar{S}_z. \quad (2.49)$$

It is also seen that no quantity akin to a group velocity can be introduced to relate energy flow and Poynting flux, as has been recently suggested [7]; in any case each waveguide mode has its own group velocity, and no global definition exists for this quantity in multimode power flow.

It can be explicitly demonstrated that the radiation power flow as given by Eq. (2.49) overcomes all four difficulties mentioned above. In Appendix B, where somewhat involved algebraic manipulations are carried out, it is shown that Eq. (2.49) can be reduced to

$$\bar{P}_z = \int_0^{2\pi} d\theta \sum_{i=1}^N \int_{R_{i-1}}^{R_i} dr r (\epsilon_i \mu_i \beta^2 - 1) S_z. \quad (2.50)$$

Invoking the orthonormalization relation [Eq. (2.11)] allows Eq. (2.50) to be cast into the remarkably simple form

$$\bar{P}_z = -cq_0^2 \beta \sum_{l=-\infty}^{\infty} \sum_{n=1}^{\infty} \frac{e_{z,n}^2(r_0)}{C_n} \Theta(-s) \equiv - \sum_{l=-\infty}^{\infty} \sum_{n=1}^{\infty} P_{ln}, \quad (2.51)$$

where C_n is given by Eq. (2.11a), and P_{ln} is the power radiated into the HEM_{ln} mode. Note the minus sign in Eq. (2.51): radiation power flows in a direction *opposite* to that of the bunch.

As claimed, the radiation power flow given by Eq. (2.51) is indeed in a form where contributions are decoupled mode by mode; this property is not enjoyed by either U or P_z . Radiation power is a function independent of s (behind the bunch), and thus free of peaks and valleys even though no average over either z or t was performed. So, as expected, the quantity \bar{P}_z is naturally uniform behind the bunch, consistent with the uniform nature of the waveguide structure wherein the radiation is propagating. Finally, if one compares Eq. (2.51) and Eq. (2.39), it is evident that

$$\bar{P}_z = v F_{z,\text{drag}}, \quad (2.52)$$

as indeed it must if the theory is to be internally consistent. Clearly, since $F_{z,\text{drag}}$ is naturally uniform, and so \bar{P}_z must also be.

G. Finite bunch length effects

We now consider effects associated with the finite length of a charge bunch. As pointed out in Sec. IIC, the only formal change in the theory to allow for this extension from a point charge source is a modification of the g functions according to the prescription given in Eq. (2.25). To simplify the discussion that follows, a rectangular charge distribution is selected, with a distribution function $f(s) = \Delta^{-1}$ if $-\Delta/2 \leq s \leq \Delta/2$, and $f(s) = 0$ otherwise. The integral in Eq. (2.25) is straightforward, yielding

$$\begin{pmatrix} g_{z,n}(s) \\ g_{\perp,n}(s) \end{pmatrix} = \frac{1}{k_n \Delta} \begin{pmatrix} \sin k_n s' \\ \cos k_n s' \end{pmatrix} \Theta(s') \Big|_{s' = -s - \Delta/2}^{s' = -s + \Delta/2}. \quad (2.53)$$

This expression can be evaluated in front of the beam, within the beam, and behind the beam, by taking into account the properties of the Heaviside function. In front of the beam $s > \Delta/2$, and one finds

$$\begin{pmatrix} g_{z,n}(s) \\ g_{\perp,n}(s) \end{pmatrix} = 0. \quad (2.54)$$

Within the beam $-\Delta/2 < s < \Delta/2$, and one finds

$$\begin{pmatrix} g_{z,n}(s) \\ g_{\perp,n}(s) \end{pmatrix} = \frac{1}{k_n \Delta} \begin{pmatrix} \sin k_n \left(-s + \frac{\Delta}{2} \right) \\ \cos k_n \left(-s + \frac{\Delta}{2} \right) - 1 \end{pmatrix}. \quad (2.55)$$

Finally, behind the beam $s < -\Delta/2$, and one finds

$$\begin{pmatrix} g_{z,n}(s) \\ g_{\perp,n}(s) \end{pmatrix} = \alpha_n(\Delta) \begin{pmatrix} g_{z,n}^0(s) \\ g_{\perp,n}^0(s) \end{pmatrix}, \quad (2.56)$$

where

$$\alpha_n(\Delta) \equiv \frac{\sin(k_n \Delta/2)}{(k_n \Delta/2)}. \quad (2.57)$$

Equation (2.54) indicates that, as expected, no fields are found ahead of the bunch. Equation (2.55) indicates that the longitudinal and transverse fields are oscillatory within the bunch, but in a conjugate relationship; this feature is responsible for the so-called head-to-tail instability of a charge bunch, in which wakefields can lead to destructive shear displacements along the bunch. Equation (2.56) indicates that the fields for a finite rectangular bunch are the same as those for a point bunch, except for the form factor $\alpha_n(\Delta)$. This factor has the effect of reducing the mode amplitudes $1/C_n$ for a point charge bunch to α_n/C_n for the distributed bunch. From the familiar properties of $\alpha_n(\Delta)$, it is seen that higher-order modes for which $k_n \Delta > \pi$ are reduced in amplitude. Those are modes with half-wavelengths less than the bunch length. This demonstrates the rather obvious point that excitation of short wavelength higher-order wakefield modes requires short drive bunches.

III. EXAMPLES

The analytic solutions obtained in previous sections of this paper using the method of eigenmode expansion have revealed a number of important features of wakefields in dielectric-lined waveguides that could not easily be revealed through other theoretical formulations. The compact and relatively transparent analytic solutions [e.g., Eqs. (2.24) and (2.35)] also permit numerical evaluations to be obtained speedily and reliably, since singularities that are endemic to wakefields have been dealt with analytically, therefore obviating the need for delicate numerical integrations. In this section, results of numerical evaluations will be shown and discussed, and several unusual basic physics points associated with wakefields will be elucidated.

In order to generate a sharp wakefield, the drive bunch must excite many high-order waveguide modes. The sharpness of the wake most critically depends on the bunch length. This fact can be seen from plots of the computed power spectrum as shown in Fig. 3. The parameters for this example are $R_1 = 0.05$ cm, $R_2 = 0.50$ cm, $\varepsilon = 9.5$, $q_0 = 2$ nC, $\gamma = 61$, $\Delta z = 0.02$ cm, and $r_0 = 0$. These parameters lead to a wakefield period of 2.63 cm, which is compatible with operation using an X-band rf linac to generate a bunch train synchronous with the wakefields. These parameters are adhered to in the balance of this paper, unless otherwise noted. Only TM_{0n} waveguide modes are excited in this case, since $r_0 = 0$. Figure 3(a) shows P_n , the power lost by the bunch to

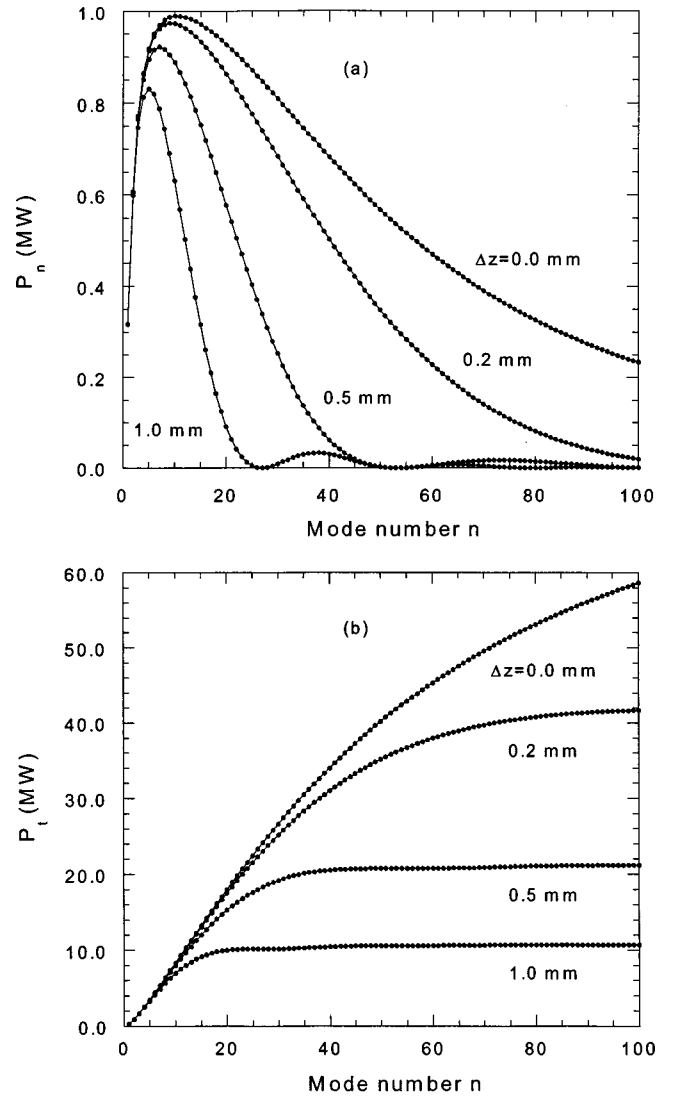


FIG. 3. Power lost by the beam to wakefields as a function of mode number n , for several values of the beam length Δz ; (a) mode spectrum, showing the power P_n lost into each mode n ; and (b) total integrated lost power in all modes up to and including the n th. As Δz is increased, the higher mode contributions diminish rapidly and the total lost power decreases. These results show that is important to use a short bunch to generate strong wakefields.

radiation, as apportioned among the TM_{0n} waveguide modes, plotted versus n . The quantity P_n is P_{ln} as given by Eq. (2.51) with $l=0$, since contributions with $l \neq 0$ vanish in this case. As the bunch length Δz grows, higher-order modes are less strongly excited, and the wake will smear out quickly. At the same time, the total lost and radiated power drop rapidly together with a diminution in drag force. Lower drag is an indication of lower acceleration gradient. A measure of the total power lost to drag forces and radiated is given by $P_t = \sum_{n'=1}^n P_{n'}$. This quantity, and its dependence upon bunch length, is shown in Fig. 3(b), also plotted versus n . It is seen that as the bunch length decreases, an increasing number of modes must be included in the calculation in order to account for all the lost and radiated power.

Mode dispersion is also a significant factor in determining the nature of wakefields. Dispersion influences such factors as peak amplitude of the fields, and spreading of the peaks at

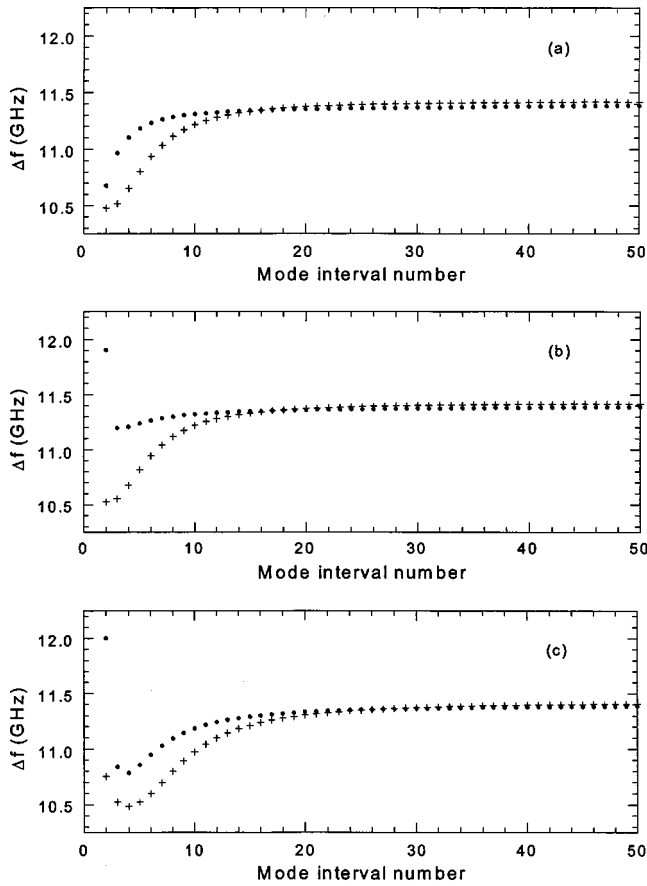


FIG. 4. Frequency separation between adjacent modes as a function of mode interval number for (a) monopole ($l=0$), (b) dipole ($l=1$), and (c) quadrupole ($l=2$) modes. The dots represent the frequency separations between (TE-like) odd- n modes, while the pluses represent frequency separations between (TM-like) even- n modes. It can easily be shown that all mode separations approach a universal asymptotic frequency separation $\Delta\omega = \pi c / [(R_2 - R_1)\sqrt{\epsilon - 1}]$, in the limit of large n ; for this example, $\Delta\omega/2\pi = 11.433$ GHz. This near equality of frequency separations is responsible for creating localized wakefields with different l values at the same z locations, as shown in Fig. 7. Therefore, it is not possible to separate the accelerating monopole field from the transverse components of the dipole field that can lead to instability. Dispersion in the modes with lower n values leads to a smearing of the wake as the distance behind the bunch increases.

increasing distances behind the bunch. Furthermore, study of stability properties of a bunch requires knowledge of the relative strength of mode amplitudes, and the relative locations of the field peaks for modes with different l values. Typically, for a dielectric loaded waveguide, the dispersion line for each mode plotted in the ω - k plane has a hyperbolic shape when k is small, but bends over to become a straight line of slope $c/\sqrt{\epsilon}$ when k is large. This leads to a nearly uniform spacing of modes in the TE and TM like families for large k . The TE-like modes have odd- n values, while the TM-like modes have even- n values. Results of computations to determine the eigenfrequencies are shown in Fig. 4, for monopole modes [$l=0$, Fig. 4(a)], dipole modes [$l=1$, Fig. 4(b)], and quadrupole modes [$l=2$, Fig. 4(c)]. Parameters are as for the results shown in Fig. 3. The figures show frequency differences between adjacent modes of the same

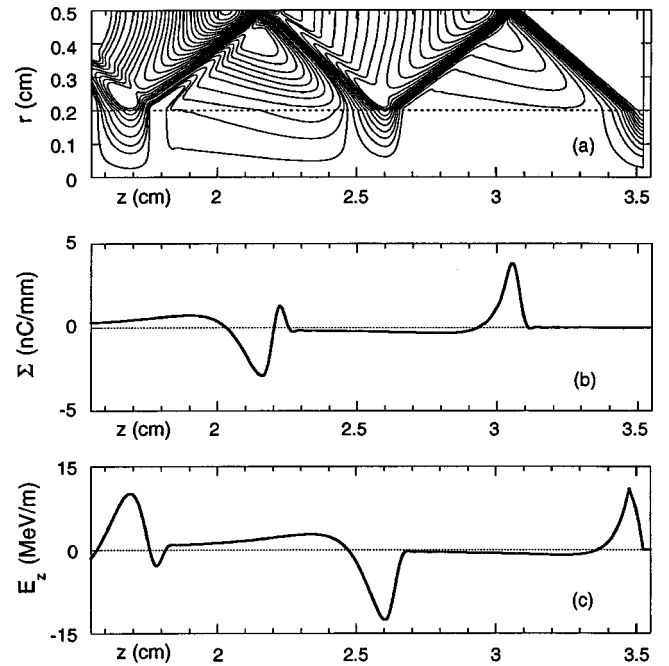


FIG. 5. An example to show the structure of wakefields in a dielectric waveguide: (a) the electric flux lines; (b) the lineal surface charge density induced on the wall of the conductor; and (c) the accelerating gradient E_z on the axis. Note that the flux appears to emerge uniformly out of a disk located at the beam position, although the beam is assumed to be a charged rod of length $\Delta z = 0.05$ cm with infinitesimal radius. The electric flux lines are bent at the dielectric boundary ($R_1 = 0.2$ cm), and terminate at the conducting wall charge ($R_2 = 0.5$ cm). Note that excess charge is induced on the wall, and acts as a source of the trailing wakefield. The dielectric constant is intentionally chosen to be low ($\epsilon = 3.0$) to show the structure of the wake lines more clearly than for the case of a higher dielectric constant, as in Fig. 6.

type, plotted as a function of like-mode interval number. The figures are qualitatively similar to one another, show significant dispersion for low mode interval numbers, but show negligible dispersion at high mode interval numbers. All mode intervals asymptotically approach the limiting value $\Delta f = c/[2(R_2 - R_1)\sqrt{\epsilon - \beta^{-2}}] = 11.433$ GHz for the parameters chosen, but the rate of approach to this asymptote is gentler for higher l . The mode dispersion at low mode interval numbers leads to spreading of the wakefield peaks as distance behind the bunch increases. However, since Fig. 3(a) shows that short bunches excite lower- n modes more weakly than intermediate- n modes, spreading is minimized for wakefields excited by short bunches. The near equality of mode intervals for monopole, dipole, and quadrupole modes indicates that transverse fields are not displaced away from the bunch location to mitigate against destabilization, as previously speculated [10].

In Fig. 5, computed wakefields and surface charges are shown. For this example, a 2-nC, 30.7-MeV ($\gamma = 61$) charge bunch with length $\Delta z = 0.05$ cm is moving uniformly along the axis in dielectric loaded waveguide. The waveguide has a vacuum hole of radius $R_1 = 0.2$ cm, a conducting boundary radius $R_2 = 0.5$ cm, and a dielectric constant $\epsilon = 3.0$. The bunch is located at $z = 3.5$ cm, and is moving toward the right. For this example, parameters were chosen to allow the

crowded wakefield pattern to be easier to discern, in contrast to cases with more highly localized wakefield features. Figure 5(a) shows the pattern of electric flux lines of the wakefields. The coordinates of the flux lines [$r(z)=\text{const}$] were obtained by numerically solving the differential equation $dr/dz=E_r/E_z$, where the fields E_r and E_z are given by Eq. (2.24). One unusual feature is that the source of flux appears to be distributed radially over a disk of radius R_1 at the location of the bunch, even though the bunch actually has a vanishing radial extent. The field (for $s<0$) is similar to that for a charged disk filling the vacuum hole. The density of flux lines is normalized such that the 2-nC bunch generates ten flux lines. The electric flux lines are refracted at the vacuum-dielectric boundary, and some of them are terminated by polarization charge. But for the sake of visualization, the plot shows the same number of the flux lines continuing into the dielectric layer. The flux lines are reflected at the conducting boundary and the trailing pattern of the wake continues.

At the wall, surface charge is induced as shown in Fig. 5(b). The lineal charge density $\Sigma(z)$ is related to the electric flux density $\Phi_w(z)$ on the wall through Gauss's law as $\Phi_w(z)=2\pi R_2 E_r(r=R_2, z)=4\pi\Sigma(z)/\epsilon$. It can be seen that excess surface charge is induced on the wall, as is necessary to act as the source of the trailing wakefield. By integrating the surface charge from the bunch back to $z=2.9$ cm, a net positive surface charge of 5.5 nC is found; this is 2.75 times that of the drive bunch charge (with opposite sign). This feature is another peculiar feature of Cerenkov radiation in a bounded system. Outside the Cerenkov regime, the total induced wall charge is equal to the source charge (with opposite sign), and there is no trailing wakefield formed.

The electric field on the axis $E_z(0, z)$, as plotted in Fig. 5(c), exhibits localized peaks with alternating signs. It is evident that the leading edge of the axial field at the drive bunch near $z=3.5$ cm is slightly bent, a consequence of finite bunch length. The field contributions arising from different elements of the bunch superimpose to give this bend, and the peak value is comparable to the second peak. If the drive bunch were a point charge, the leading edge of the first peak would go its maximum immediately, and its height would be roughly half that of the first negative peak. This factor of $\frac{1}{2}$ would be consistent with Wilson's theorem [9]; but here it is seen that the conditions for validity of the theorem are violated for finite bunch length, even though $\Delta z=0.05$ cm is clearly smaller than any other dimension of the system. Multiple drive bunches can be used to enhance the accelerating field by carefully choosing their spacing to coincide with the positive peaks, and acceleration of a test bunch occurs at locations of negative peaks [3]. Discussion of wakefields from multiple drive bunches are beyond the scope of this paper.

In Fig. 6, a wakefield flux pattern is depicted for parameters that are optimized for high acceleration gradient. Here $R_1=0.05$ cm, $R_2=0.15$ cm, $\epsilon=9.5$, $q_0=2$ nC, $\gamma=61$, and $\Delta z=0.02$ cm. In this case, it is seen that the wake is much sharper than that shown in Fig. 5(a). The Cerenkov cone is clearly in evidence. It can be easily verified that the cone angle is essentially that for Cerenkov radiation in an unbounded medium, i.e., $\cos^{-1}(1/\epsilon\beta)\approx 84^\circ$. The peak accelerating field on axis at $z=1.85$ cm in this case is 155 MeV/m.

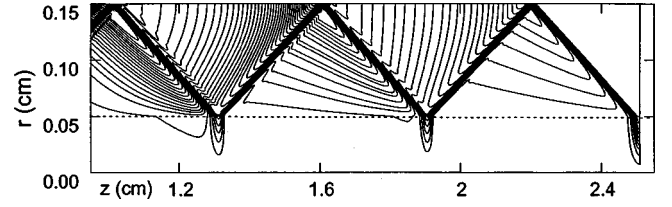


FIG. 6. Wakefield flux lines for a more realistic case than that in Fig. 5. Here $R_1=0.05$ cm, $R_2=0.15$ cm, $\epsilon=9.5$, and $\Delta z=0.02$ cm. Note that the wake is much sharper than the case shown in Fig. 5, and clearly illustrates the qualitative notion that the outer conducting boundary serves to periodically reflect the Cerenkov cone back toward the axis. The cone angle closely agrees with the customary value $\cos^{-1}(1/\epsilon\beta)$ for Cerenkov radiation in an unbounded system.

In Fig. 7, the forces acting on a test bunch of unit charge trailing a 2-nC drive bunch are shown, as a function of the distance behind the drive bunch. The parameters of the waveguide and the drive bunch are chosen identical to those as in Fig. 3, except that the drive bunch is now moving parallel to but displaced from the axis by $r_0=0.010$ cm in the x direction. This radial displacement produces azimuthally asymmetric modes ($l\neq 0$), in addition to the symmetric ones ($l=0$). Figures 7(b) and 7(d) show the longitudinal and transverse fields near the drive bunch, whose axial extent is indicated by the filled rectangle; while Figs. 7(a) and 7(c) show the fields near the location for a test bunch, indicated by the open rectangle. The longitudinal force F_z , as shown in Figs. 7(a) and 7(b), acts either to accelerate or decelerate elements of the test bunch, depending on its sign. The transverse forces F_x , as shown in Figs. 7(c) and 7(d), is responsible for the stability of the test charge. It is assumed that the test charge is also displaced in the x direction by 0.01 cm. Since the dipole force is the main component of concern regarding the stability, and since it is uniform over the cross section of the vacuum hole, the test particle is always accelerated radially in the same direction as the displacement of the drive bunch. For ease of comparison, the plots in Figs. 7(a)–7(d) show the dipole force multiplied by a factor of 10, and the quadrupole force multiplied by a factor of 100. From Fig. 7(a) it is apparent that the drag force on each part of the bunch is different, and thus different segments of a bunch with finite length will lose different amounts of energy. If the beam were a point charge, the average drag force would be half of the accelerating force shown in Fig. 7(a), a limiting circumstance that is the basis of Wilson's theorem [9]. But in the example shown here the beam length is finite, and the drag force builds up to more than half the accelerating force. It is also apparent from Figs. 7(c) and 7(d) that both the accelerating bunch and the drive bunch are in regions where the transverse force varies rapidly. As a result, a finite length beam will tend to distort into a banana shape. This unavoidable feature is intrinsic to wakefields, as a consequence of the Panofsky-Wenzel theorem [8].

A comparison, near the location of a test bunch, between the transverse force shown in Fig. 7(c) with the longitudinal force shown in Fig. 7(a), reveals their ratio to be about 1/10. Considering the small radius of the waveguide and the fact that the dipole force increases in proportion to the deviation from the axis, it is clear one must either keep the drive beam

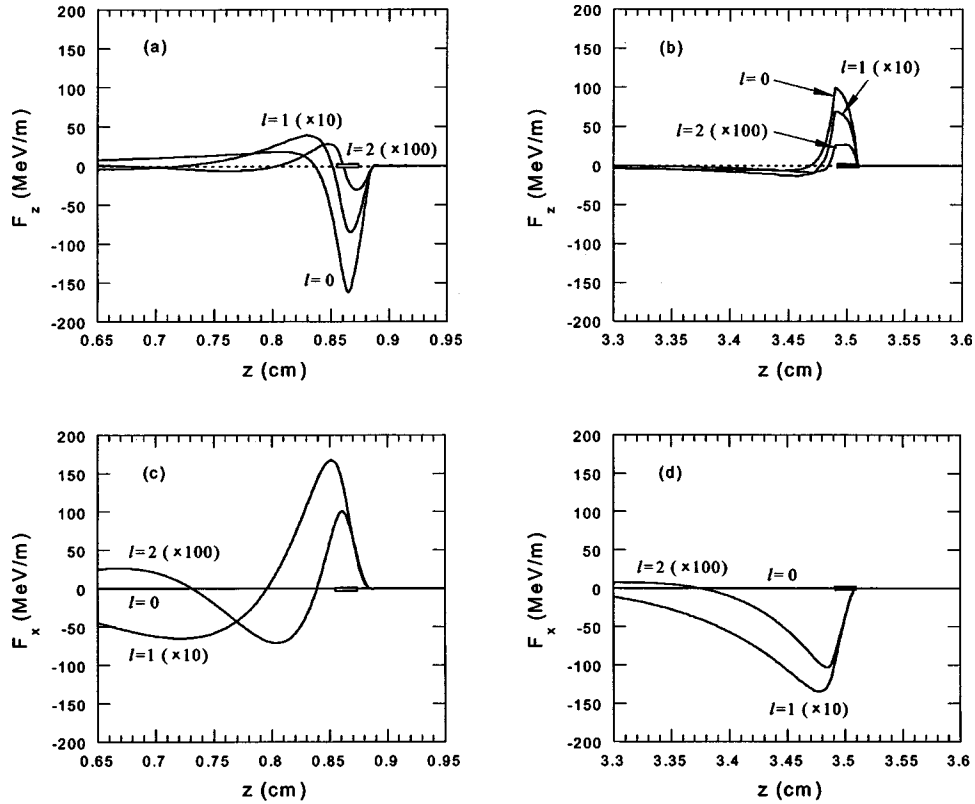


FIG. 7. Forces on a test particle with unit charge following a 2 nC, $\Delta z = 0.02$ cm drive bunch for monopole, dipole, and quadrupole fields. These fields are generated by the drive bunch moving parallel to the axis, but displaced in the x direction by an increment $r_0 = 0.01$ cm, in a waveguide with $R_1 = 0.05$ cm, $R_2 = 0.50$ cm, and $\epsilon = 9.5$. For the sake of clarity, the dipole force ($l = 1$) is multiplied by factor of 10, and the quadrupole force ($l = 2$) is multiplied by a factor of 100. (a) Longitudinal forces near the first accelerating peak, where the location of a would-be accelerating bunch is indicated by the open box at the peak of the main accelerating force. Note that the dominant contribution to the accelerating gradient is from the $l = 0$ component. (b) Longitudinal forces near the drive bunch. (c) Transverse forces near the first accelerating peak. Note that different parts of the would-be accelerating test bunch will experience quite different transverse forces, leading to a head-to-tail instability that will result in a banana-shaped bunch. (d) Transverse forces near the drive bunch. Again, head-to-tail instability is evident.

close to the axis, or keep the dielectric waveguide short. Therefore, it appears necessary to employ strong focusing to minimize deviations of the beam from the axis, and/or to evolve a scheme with short waveguide modules having high wakefield gradients. Further discussion on bunch stability, focusing and use of short (cavity) dielectric resonator accelerating modules is beyond the scope of this paper.

Figure 8 illustrates important issues in regard to the distinction in the wakefield context between radiation power and mere convection energy of the Coulomb fields. These issues are intrinsic for any convecting system, such as in the case of wakefields from a charge bunch. Figure 8(a) shows the usual power flow P_z calculated using the customary Poynting vector; this quantity is seen to be nonuniform, with distinct peaks where the wakefield is peaked on axis. Note also that these peaks also coincide with either the location of the drive beam or the peaks of the induced wall charge at the boundary of the dielectric. These locations are where one can also expect strong Coulomb fields. In Fig. 8(b), the convected energy vU is shown; this quantity includes both the radiation energy and the convecting Coulomb energy. It also shows distinct peaks similar to those in Fig. 8(a). Figure 8(c) shows the difference between Figs. 8(a) and 8(b), namely, $P_z - vU$, which was identified as the true radiation field P_{rad} in Sec. II. It is clear that all the peaks are essentially can-

celed, thereby resulting in a uniform flow of radiation. Note also that the sign of P_{rad} is negative, indicating that the radiation power flow is opposite to the directions of the bunch motion, of P_z and of vU . To our knowledge, this fundamental distinction has not been previously noted.

IV. DISCUSSION

In this paper, a derivation is presented for the general analytic solution using the method of eigenfunction expansion for wakefields induced by a charge bunch moving parallel to the axis of a cylindrical dielectric-lined channel. Wakefields, equivalent to Cerenkov radiation in a bounded system, are electromagnetic shock waves similar to Mach waves in acoustic systems: they contain a singularity at the wake front. Because of this singularity, and the fact that the fields of greatest interest are highly concentrated in a narrow region, a purely numerical approach to solve Maxwell's equations with a moving source is computationally intensive and susceptible to error. An analytic solution, on the other hand, allows straightforward checks of the accuracy to be carried out, such as consistency with Gauss's law. A wakefield solution in terms of orthonormal eigenfunctions also leads to intuitively satisfying and remarkably compact expressions for the forces experienced by drive and test

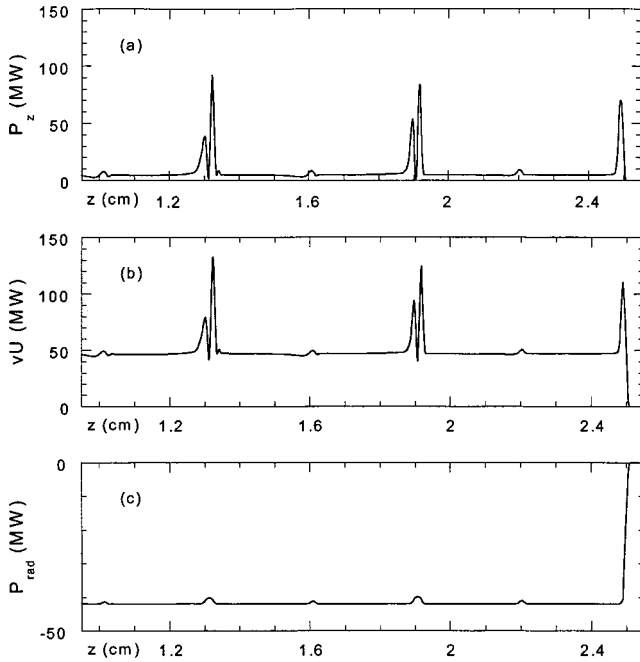


FIG. 8. Three different types of energy flow associated with wakefields of a moving source. (a) Power flow P_z , as calculated from the Poynting vector. Note that this power flow is not uniform but is highly peaked, particularly near the peaks of the wakefield on the axis. This power flow includes a contribution from the electrostatic Coulomb field energy affixed to the charge. (b) Convecting energy flow vU . (c) The difference $P_z - vU$, representing the true radiated power P_{rad} . Note that the magnitude of P_{rad} is uniform in z , and that its sign is negative, indicating that it flows backwards, i.e., receding away from the moving source.

bunches, and for the power radiated by a drive bunch. Analytical consistency of the solution with the Panofsky-Wenzel theorem [8] and with Wilson's theorem [9] is also straightforward to establish.

There have been attempts to solve for wakefields in a dielectric waveguide by the method of direct integration of the Green's function [4,5]. In this approach, an analytic expression for the fields can be obtained in terms of a sum of residues over an infinite number of poles, each corresponding to an eigenmode. However, this kind of solution is useful only when the system is not bounded or when only a few modes are adequate, because the residues must each be found by numerically differentiating the dispersion relation at each pole. As seen in Sec. III, over 100 modes can be required to describe accurately a relatively sharp wakefield. Although the prescription for evaluating the residues at the poles is given, no explicit form is available. Thus this type of solution can be cumbersome to use for obtaining numerical results, does not shed light on the physical nature of the wakefield, and does not lead naturally to the consistency checks mentioned above.

In order to apply the method of eigenfunction expansion, it is essential to have an orthonormality relation to solve for mode amplitudes. For a cylindrical waveguide loaded with concentric dielectric layers, it seems that no such general relation had until now appeared in the literature, except for azimuthally symmetric modes [11]. Due to the nature of a structure with multiply connected regions, the available ar-

gument to prove orthonormality [12] does not apply. In this paper a generalized orthonormality relation is derived for the first time, to our knowledge, both for a stationary source and for a convected source such as a charge bunch moving along a dielectric-loaded waveguide. Since the orthogonality relation is in an explicit form, it is straightforward to calculate numerical values for the fields, and also to clarify many related physical issues, as shown in Sec. II.

Another point discussed in this paper stems from the fact that a uniformly moving charge bunch in a dielectric-lined waveguide is a convecting system, rather than a stationary system such as a linear microwave tube. This fact requires care in deriving an appropriate orthogonality relation, as mentioned above and shown in Sec. II B. Another feature peculiar to a convecting system is in regard to radiated power. In Sec. II F and as shown in Fig. 8, it is erroneous in a convecting system to interpret the Poynting vector as radiation power. In a convecting system, Coulomb field energy appears as a power flow that contributes to the Poynting vector. Therefore, as is shown in this paper, for the first time to our knowledge, one must subtract this contribution from the Poynting vector to obtain the true radiation power. We have shown that the radiation power is uniform behind the bunch, and is flowing backward away from the source; indeed, causality prevents radiation from flowing forward. It has also been shown in this paper that the radiation power is equal, as it must be, to the work done by the self-drag force which, for a point charge, is consistent with Wilson's theorem [9]. Furthermore, we have shown that this radiation power flow can be decoupled into individual waveguide modes, while the Poynting vector cannot. The final analytical expression for the radiated power [Eq. (2.51)] is a remarkably simple form.

The condition for nonvanishing of the radiation power P_{rad} coincides with the condition for generation of Cerenkov radiation, namely, $\beta^2 \epsilon > 1$. When this condition is met, the solution of the wave equation goes to a shock wave solution. The transition into the Cerenkov regime introduces several interesting features that are fundamentally different from ordinary wave solutions. (i) The wake possesses a sharp discontinuous front, such that the field vanishes ahead of it. (ii) This feature is the result of the causality condition, which is imposed for evaluation of a contour integral by requiring both poles to lie in the lower-half plane of the complex k plane, as shown in Fig. 1. (iii) The wake front in the dielectric region is bent backward at the Cerenkov angle $\cos^{-1}(1/\epsilon\beta)$, as shown in Figs. 5 and 6. (iv) Excess wall charge is induced on the conducting boundary, which acts as the source of the trailing wake, as shown in Fig. 5.

Analysis of the power spectrum in a wakefield shows that it is necessary to use a short bunch in order to produce a sharp wake. A sharper wake implies less dispersion, and a higher accelerating gradient. A less dispersive wake is crucial for applications using multiple drive bunches, either in a waveguide or a cavity configuration. From the examples shown in Sec. III, it would not appear to be unreasonable to design and build a wakefield accelerator with an acceleration gradient of 150 MeV/m or more.

Of course, the usefulness of the wakefields to provide high gradient acceleration depends critically on the stability of the drive and test bunches. The solution obtained in this

paper provides the means to calculate transverse and longitudinal forces on a nonaxisymmetric bunch. The analytic form of the solution presented allows a remarkably simple form of the force to be obtained, which checks with the Panofsky-Wenzel theorem. The consequence of this theorem is that one cannot separate stability problem from achievement of a high accelerating gradient, a condition that prevails in any accelerating structure. It is also shown that the force vector can be derived as the gradient of a pseudopotential. The accelerating gradient depends sensitively on the vacuum hole size. However, use of a small hole exacerbates the stability issue, since any but very small deviations from axisymmetry are intolerable. It has also been shown that peaks of the dipole fields overlap peaks of the longitudinal field. This requires that a compromise be reached between achievement of a high accelerating gradient and achievement of bunch stability. Of course, the transverse forces vanish when the drive bunch moves to the waveguide axis, and therefore it is critically important to study stability with an external focusing force, such as can be provided by quadrupole magnets. Our analytic solution presented in this paper will provide an essential tool for such a study.

Future steps to be undertaken in the quest to understand and employ wakefields for acceleration include use of a multibunch drive train, use of a short dielectric resonator, and use of external beam focusing to provide stability.

ACKNOWLEDGMENTS

Appreciation for stimulating and helpful discussions is extended to T. C. Marshall, T.-B. Zhang, V. P. Yakovlev, W. Gai, and J. G. Power. Help in preparation of the figures by M. A. LaPointe and Changbiao Wang is acknowledged, as is a careful reading of the manuscript by A. K. Ganguly. This research was supported in part by the U.S. Department of Energy.

APPENDIX A: GENERALIZED ORTHONORMALITY RELATION

Consider the following overlap integral between radial eigenfunctions for two different modes:

$$\Psi_{mn}^{(i)} = \int_{R_{i-1}}^{R_i} dr r [e_{r,m}(r)h_{\theta,n}(r) + e_{\theta,m}(r)h_{r,n}(r)], \quad (\text{A1})$$

where the modes have transverse wave numbers

$$k_{\perp,m}^2 = \varepsilon_j \mu_i \frac{\omega_m^2}{c^2} - k_m^2 \quad \text{and} \quad k_{\perp,n}^2 = \varepsilon_i \mu_i \frac{\omega_n^2}{c^2} - k_n^2, \quad (\text{A2})$$

and (ω_m, k_m) and (ω_n, k_n) represent two arbitrary points that satisfy the dispersion relation Eq. (2.8). Using Eq. (2.3), one can write Eq. (A1) as

$$\begin{aligned} \Psi_{mn}^{(i)} = & \frac{1}{k_{\perp,m}^2 k_{\perp,n}^2} \int_{R_{i-1}}^{R_i} dr r \left\{ k_m k_n \frac{l}{r} \frac{d}{dr} (e_{z,m} h_{z,n}) \right. \\ & + \varepsilon_i \mu_i \frac{\omega_m}{c} \frac{\omega_n}{c} \frac{l}{r} \frac{d}{dr} (h_{z,m} e_{z,n}) + k_m \varepsilon_i \frac{\omega_n}{c} \left(\frac{de_{z,m}}{dr} \frac{de_{z,n}}{dr} \right. \\ & + \frac{l^2}{r^2} e_{z,m} e_{z,n} \left. \right) + k_n \mu_i \frac{\omega_m}{c} \left(\frac{dh_{z,m}}{dr} \frac{dh_{z,n}}{dr} \right. \\ & \left. \left. + \frac{l^2}{r^2} h_{z,m} h_{z,n} \right) \right\}. \quad (\text{A3}) \end{aligned}$$

The first two terms are already in the form of total derivatives. The first parts of the third and the fourth terms can be integrated by parts, and then the differential equation (2.2) can be used to obtain

$$\begin{aligned} k_{\perp,m}^2 k_{\perp,n}^2 \Psi_{mn}^{(i)} = & \left[k_m k_n l e_{z,m} h_{z,n} + \varepsilon_i \mu_i \frac{\omega_m}{c} \frac{\omega_n}{c} l h_{z,m} e_{z,n} \right. \\ & + \varepsilon_i k_m \frac{\omega_n}{c} r e_{z,m} \frac{de_{z,n}}{dr} \\ & \left. + \mu_i k_n \frac{\omega_m}{c} r h_{z,m} \frac{dh_{z,n}}{dr} \right]_{R_{i-1}}^{R_i} \\ & + \varepsilon_i k_m k_{\perp,n}^2 \frac{\omega_n}{c} \int_{R_{i-1}}^{R_i} dr r e_{z,m} e_{z,n} \\ & + \mu_i k_n k_{\perp,m}^2 \frac{\omega_m}{c} \int_{R_{i-1}}^{R_i} dr r h_{z,m} h_{z,n}. \quad (\text{A4}) \end{aligned}$$

The last two remaining integrals in Eq. (A4) are performed as follows. Equation (2.2) is recast as

$$\frac{1}{r} \frac{d}{dr} \left(r \frac{de_{z,n}}{dr} \right) + \left(k_{\perp,n}^2 - \frac{l^2}{r^2} \right) e_{z,n} = 0. \quad (\text{A5})$$

For $n \neq m$, one multiplies Eq. (A4) by $e_{z,m}$, and subtracts a similar equation with m and n interchanged. This yields

$$\begin{aligned} (k_{\perp,m}^2 - k_{\perp,n}^2) \int_{R_{i-1}}^{R_i} dr r e_{z,m} e_{z,n} \\ = \left[r e_{z,m} \frac{de_{z,n}}{dr} - r e_{z,n} \frac{de_{z,m}}{dr} \right]_{R_{i-1}}^{R_i}, \quad (\text{A6}) \end{aligned}$$

and, similarly,

$$\begin{aligned} (k_{\perp,m}^2 - k_{\perp,n}^2) \int_{R_{i-1}}^{R_i} dr r h_{z,m} h_{z,n} \\ = \left[r h_{z,m} \frac{dh_{z,n}}{dr} - r h_{z,n} \frac{dh_{z,m}}{dr} \right]_{R_{i-1}}^{R_i}. \quad (\text{A7}) \end{aligned}$$

Employing Eqs. (A6) and (A7), rearranging, and making use of Eq. (2.3), leads to

$$(k_{\perp m}^2 - k_{\perp n}^2) \Psi_{mn}^{(i)} = \left\{ r \left[\left(k_m e_{z,m} h_{\theta,n} + \mu_i \frac{\omega_m}{c} h_{z,m} h_{r,n} \right) - \left(k_n e_{\theta,m} h_{z,n} + \varepsilon_i \frac{\omega_n}{c} e_{z,m} e_{r,n} \right) \right] \right\}_{R_{i-1}}^{R_i} \cdot \sum_{i=1}^N \Psi_{mn}^{(i)} = \delta_{mn} C'_n, \quad (\text{A14})$$

with $\Psi_{mn}^{(i)}$ as given by Eq. (A12).

When the source is moving with constant velocity and excited modes satisfy the relation $\omega_m = k_m v$, as for Cerenkov radiation in the dielectric-lined waveguide, orthogonality takes a form different from Eq. (A13). This follows since $(k_m^{(i)})^2 = k_m^2 (\varepsilon_i \mu_i \beta^2 - 1)$ is a quantity which varies from layer to layer. Thus

$$(k_m^2 - k_n^2) \sum_{i=1}^N (\varepsilon_i \mu_i \beta^2 - 1) \Psi_{mn}^{(i)} = 0 \quad \text{for } m \neq n, \quad (\text{A15})$$

Equation (A8) is written in terms of quantities for which it is convenient to apply boundary conditions, such as the continuity of $(e_z, h_z, e_\theta, h_\theta, \varepsilon e_r, \mu h_r)$ at a dielectric interface, and the vanishing of (e_z, h_r, e_θ) at the conducting wall. Applying these boundary conditions leads directly to

$$\sum_{i=1}^N (k_{\perp m}^2 - k_{\perp n}^2) \Psi_{mn}^{(i)} = 0 \quad \text{for } n \neq m. \quad (\text{A9})$$

This is the generalized orthogonality relation. For $n = m$, a different procedure is required to carry out the integrals in Eq. (A4). One multiplies Eq. (A5) by $r^2 (de_{z,n}/dr)$, and integrates by parts, to obtain

$$k_{\perp n}^2 \int_{R_{i-1}}^{R_i} dr r e_{z,n}^2 = \left\{ \frac{r^2}{2} \left[\left(\frac{de_{z,n}}{dr} \right)^2 + \left(k_{\perp n}^2 - \frac{l^2}{r^2} \right) e_{z,n}^2 \right] \right\}_{R_{i-1}}^{R_i}, \quad (\text{A10})$$

and, similarly,

$$k_{\perp n}^2 \int_{R_{i-1}}^{R_i} dr r h_{z,n}^2 = \left\{ \frac{r^2}{2} \left[\left(\frac{dh_{z,n}}{dr} \right)^2 + \left(k_{\perp n}^2 - \frac{l^2}{r^2} \right) h_{z,n}^2 \right] \right\}_{R_{i-1}}^{R_i}. \quad (\text{A11})$$

Substituting these into Eq. (A4), one obtains

$$k_{\perp n}^4 \Psi_{nn}^{(i)} = \left\{ \left(k_n^2 + \mu_i \varepsilon_i \frac{\omega_n^2}{c^2} \right) l e_{z,n} h_{z,n} + \varepsilon_i k_n \frac{\omega_n}{c} \right. \\ \times \left[r e_{z,n} \frac{de_{z,n}}{dr} + \frac{r^2}{2} \left(\left(\frac{de_{z,n}}{dr} \right)^2 + \left(k_{\perp n}^2 - \frac{l^2}{r^2} \right) e_{z,n}^2 \right) \right] \\ + \mu_i k_n \frac{\omega_n}{c} \left[r h_{z,n} \frac{dh_{z,n}}{dr} + \frac{r^2}{2} \left(\left(\frac{dh_{z,n}}{dr} \right)^2 + \left(k_{\perp n}^2 - \frac{l^2}{r^2} \right) h_{z,n}^2 \right) \right] \left. \right\}_{R_{i-1}}^{R_i}, \quad (\text{A12})$$

which can be used to calculate the normalization constant.

Two particular cases are of interest, namely, that of a stationary source where it is legitimate to set $\omega_m = \omega_n$, and that of a moving charge bunch as a source where it is necessary to set $\omega_m = k_m v$. In the first instance, Eq. (A9) reduces to

$$(k_m^2 - k_n^2) \sum_{i=1}^N \Psi_{mn}^{(i)} = 0 \quad \text{for } m \neq n, \quad (\text{A13})$$

from which, since $k_m^2 \neq k_n^2$, the orthonormality relation for stationary sources is found, namely,

since $k_m^2 \neq k_n^2$. Therefore, one obtains the relevant orthonormality relation

$$\sum_{i=1}^N (\mu_i \varepsilon_i \beta^2 - 1) \Psi_{mn}^{(i)} = \delta_{mn} C_n, \quad (\text{A16})$$

so that

$$C_n = \sum_{i=1}^N (\mu_i \varepsilon_i \beta^2 - 1) \Psi_{nn}^{(i)}, \quad (\text{A17})$$

with, as above, $\Psi_{nn}^{(i)}$ given by Eq. (A12). However, in this case the form of Eq. (A12) can be simplified somewhat by expressing the first terms in the second and third brackets in terms of $h_{\theta,n}$ and $e_{\theta,n}$, and by invoking boundary conditions. As a result, the following form for C_n is found.

$$C_n = \sum_{i=1}^N \left\{ \frac{r^2}{2} \varepsilon_i \left[\frac{1}{k_{\perp n}^2} \left(\frac{de_{z,n}}{dr} \right)^2 + \left(1 - \frac{l^2}{k_{\perp n}^2 r^2} \right) e_{z,n}^2 \right] \right. \\ \left. + \mu_i \left[\frac{1}{k_{\perp n}^2} \left(\frac{dh_{z,n}}{dr} \right)^2 + \left(1 - \frac{l^2}{k_{\perp n}^2 r^2} \right) h_{z,n}^2 \right] \right\}_{R_{i-1}}^{R_i}. \quad (\text{A18})$$

For finding the orthonormality relation in the case of wakefields when $\omega_m = \beta c k_m$, an alternative form can be derived that is less cumbersome to compute than is Eq. (A18). This form is found from Eq. (A4), using the relations between field components as given from Eq. (2.3), namely

$$\varepsilon \frac{\omega_n}{c} \frac{de_{z,n}}{dr} = k_{\perp,n}^2 h_{\theta,n} - k_n \frac{l}{r} h_{z,n}, \quad (\text{A19})$$

$$\mu \frac{\omega_n}{c} \frac{dh_{z,n}}{dr} = k_{\perp,n}^2 e_{\theta,n} - k_n \frac{l}{r} e_{z,n},$$

to obtain

$$\begin{aligned}
k_{\perp,n}^2 \Psi_{mn}^{(i)} &= \left[r k_m e_{z,m} h_{\theta,n} + r \frac{\omega_m}{\omega_n} h_{z,m} \left(k_n e_{\theta,n} + \frac{l}{r} e_{z,n} \right) \right]_{R_{i-1}}^{R_i} \\
&+ \int_{R_{i-1}}^{R_i} dr r \left(k_m \frac{\omega_n}{c} \varepsilon_i e_{z,m} e_{z,n} \right. \\
&\left. + k_n \frac{\omega_m}{c} \mu_i h_{z,m} h_{z,n} \right). \quad (\text{A20})
\end{aligned}$$

The quantities in square brackets in Eq. (A20) vanish upon summation over layers. Thus one obtains

$$\begin{aligned}
\sum_{i=1}^N k_{\perp,m}^2 \Psi_{mn}^{(i)} &= \sum_{i=1}^N \int_{R_{i-1}}^{R_i} dr r \\
&\times \left(k_m \frac{\omega_n}{c} \varepsilon_i e_{z,m} e_{z,n} + k_n \frac{\omega_m}{c} \mu_i h_{z,m} h_{z,n} \right). \quad (\text{A21})
\end{aligned}$$

Now, for the wakefield case, one has $k_{\perp,m}^2 = (\varepsilon_i \mu_i \beta^2 - 1) k_m^2$. Thus, employing Eqs. (A16) and (A20) leads to the relatively simple alternative form for the orthogonality relationship:

$$\begin{aligned}
\sum_{i=1}^N \int_{R_{i-1}}^{R_i} dr r \left(k_m \frac{\omega_n}{c} \varepsilon_i e_{z,m} e_{z,n} + k_n \frac{\omega_m}{c} \mu_i h_{z,m} h_{z,n} \right) \\
= C_n \delta_{mn}. \quad (\text{A22})
\end{aligned}$$

As stated in the text, it is this form that was used in Sec. II C to solve the wave equation with a source term.

APPENDIX B: POWER FLOW

In this appendix, we shall calculate the radiation power flow \bar{P}_z as defined by Eq. (2.49). The algebra is lengthy but straightforward, and the result that emerges is surprisingly simple. Substituting the fields from Eq. (2.24) into Eq. (2.49), and carrying out the elementary integration over θ , yields

$$\begin{aligned}
\bar{P}_z &= 2c q_0^2 \sum_{l=-\infty}^{\infty} \sum_{n,n'=1}^{\infty} \sum_{i=1}^N \frac{e_{z,n}(r_0) e_{z,n'}(r)}{C_n C_{n'}} \\
&\times \left[\bar{\Psi}_{n,n'}^{(i)} g_{\perp,n}^0(s) g_{\perp,n'}^0(s) - \frac{\beta}{2} \Phi_{n,n'}^{(i)} g_{z,n}^0(s) g_{z,n'}^0(s) \right], \quad (\text{B1})
\end{aligned}$$

where

$$\begin{aligned}
\bar{\Psi}_{n'}^{(i)} &\equiv \Psi_{n,n'}^{(i)} - \frac{\beta}{2} V_{n,n'}^{(i)}, \\
\Psi_{n,n'}^{(i)} &\equiv \int_{R_{i-1}}^{R_i} dr r [e_{r,n}(r) h_{\theta,n'}(r) + e_{\theta,n}(r) h_{r,n'}(r)], \\
V_{n,n'}^{(i)} &\equiv V_{e;n,n'}^{(i)} + V_{h;n,n'}^{(i)}, \quad (\text{B2}) \\
V_{e;n,n'}^{(i)} &\equiv \int_{R_{i-1}}^{R_i} dr r \varepsilon_i [e_{r,n}(r) e_{r,n'}(r) + e_{\theta,n}(r) e_{\theta,n'}(r)], \\
V_{h;n,n'}^{(i)} &\equiv \int_{R_{i-1}}^{R_i} dr r \mu_i [h_{r,n}(r) h_{r,n'}(r) + h_{\theta,n}(r) h_{\theta,n'}(r)], \\
\Phi_{n,n'}^{(i)} &\equiv \int_{R_{i-1}}^{R_i} dr r [\varepsilon_i e_{z,n}(r) e_{z,n'}(r) + \mu_i h_{z,n}(r) h_{z,n'}(r)].
\end{aligned}$$

The first quantity $\Psi_{n,n'}^{(i)}$ was obtained in Eq. (A4) and, since $\omega_n/c = k_n \beta$, it can be written as

$$\begin{aligned}
\Psi_{n,n'}^{(i)} &= \frac{k_n}{k_{\perp,n}^2} \frac{k_{n'}}{k_{\perp,n'}^2} \left\{ \left[l (e_{z,n} h_{z,n'} + \varepsilon_i \mu_i h_{z,n} e_{z,n'}) \right. \right. \\
&+ \beta r \left(\varepsilon_i \frac{de_{z,n}}{dr} e_{z,n'} + \mu_i \frac{dh_{z,n}}{dr} h_{z,n'} \right) \left. \right]_{R_{i-1}}^{R_i} \\
&+ \beta k_{\perp,n}^2 \Phi_{n,n'}^{(i)} \left. \right\}. \quad (\text{B3})
\end{aligned}$$

Next we consider $V_{e;n,n'}^{(i)}$. The integration over r can be carried as in Appendix A. Using Eq. (2.3), this quantity can be written

$$\begin{aligned}
V_{e;n,n'}^{(i)} &= \varepsilon_i \frac{k_n}{k_{\perp,n}^2} \frac{k_{n'}}{k_{\perp,n'}^2} \int_{R_{i-1}}^{R_i} dr r \left\{ \mu_i \beta \frac{l}{r} \frac{d}{dr} (e_{z,n} h_{z,n'} \right. \\
&+ h_{z,n} e_{z,n'}) + \left(\frac{de_{z,n}}{dr} \frac{de_{z,n'}}{dr} + \frac{l^2}{r^2} e_{z,n} e_{z,n'} \right) \\
&+ \left. \mu_i^2 \beta^2 \left(\frac{dh_{z,n}}{dr} \frac{dh_{z,n'}}{dr} + \frac{l^2}{r^2} h_{z,n} h_{z,n'} \right) \right\}. \quad (\text{B4})
\end{aligned}$$

The second and third terms in Eq. (B3) can be integrated by parts, and Eq. (2.2) can be used to obtain

$$\begin{aligned}
V_{e;n,n'}^{(i)} &= \varepsilon_i \frac{k_n}{k_{\perp,n}^2} \frac{k_{n'}}{k_{\perp,n'}^2} \left\{ \left[\mu_i \beta l (e_{z,n} h_{z,n'} + h_{z,n} e_{z,n'}) \right. \right. \\
&+ r \frac{de_{z,n}}{dr} e_{z,n'} + \mu_i^2 \beta^2 r \frac{dh_{z,n}}{dr} h_{z,n'} \left. \right]_{R_{i-1}}^{R_i} \\
&+ k_{\perp,n}^2 \int_{R_{i-1}}^{R_i} dr r (e_{z,n} e_{z,n'} + \mu_i^2 \beta^2 h_{z,n} h_{z,n'}) \left. \right\}. \quad (\text{B5})
\end{aligned}$$

Then $V_{h;n,n'}^{(i)}$ can be obtained from Eq. (B5) by interchanging $(\varepsilon_i \leftrightarrow \mu_i)$ and $(e \leftrightarrow h)$. Combining, we obtain

$$\begin{aligned}
V_{n,n'}^{(i)} &= \frac{k_n}{k_{\perp,n}^2} \frac{k_{n'}}{k_{\perp,n'}^2} \left\{ \left[2 \varepsilon_i \mu_i \beta l (e_{z,n} h_{z,n'} + h_{z,n} e_{z,n'}) \right. \right. \\
&+ (1 + \varepsilon_i \mu_i \beta^2) r \left(\varepsilon_i \frac{de_{z,n}}{dr} e_{z,n'} + \mu_i \frac{dh_{z,n}}{dr} h_{z,n'} \right) \left. \right]_{R_{i-1}}^{R_i} \\
&+ k_{\perp,n}^2 (1 + \varepsilon_i \mu_i \beta^2) \Phi_{n,n'}^{(i)} \left. \right\}. \quad (\text{B6})
\end{aligned}$$

Now, from Eqs. (B1) and (B5) one obtains

$$\bar{\Psi}_{n,n'}^{(i)} = \frac{k_n}{k_{\perp,n}^2} \frac{k_{n'}}{k_{\perp,n'}^2} \frac{1 - \epsilon_i \mu_i}{2} \left\{ \left[2l e_{z,n} h_{z,n'} + k_{\perp,n}^2 \beta \Phi_{n,n'}^{(i)} \right]_{R_{i-1}}^{R_i} + \beta r \left(\frac{d e_{z,n}}{d r} e_{z,n'} + \frac{d h_{z,n}}{d r} h_{z,n'} \right) \right\}. \quad (\text{B7})$$

The derivative terms may be eliminated using

$$\epsilon_i \beta \frac{d e_{z,n}}{d r} = \frac{k_{\perp,n}^2}{k_n} h_{\theta,n} - \frac{l}{r} h_{z,n},$$

$$\mu_i \beta \frac{d h_{z,n}}{d r} = \frac{k_{\perp,n}^2}{k_n} e_{\theta,n} - \frac{l}{r} e_{z,n},$$

so that one finally obtains

$$\bar{\Psi}_{n,n'}^{(i)} = -\frac{1}{2k_{n'}} \left\{ r (h_{\theta,n} e_{z,n'} + e_{\theta,n} h_{z,n'}) + \frac{k_n l}{k_{\perp,n}^2} (e_{z,n} h_{z,n'} - h_{z,n} e_{z,n'}) \right\}_{R_{i-1}}^{R_i} + k_n \beta \Phi_{n,n'}^{(i)}. \quad (\text{B8})$$

Applying the continuity conditions and vanishing at the conducting boundary on the fields, the first term in Eq. (B8) vanishes upon summation over layers. As a consequence, Eq. (B1) becomes

$$\bar{P}_z = 2c q_0^2 \sum_{l=-\infty}^{\infty} \sum_{n,n'=1}^{\infty} \frac{e_{z,n}(r_0) e_{z,n'}(r_0)}{C_n C_{n'}} \times \left\{ \left[\Lambda_{n,n'} + \frac{\beta}{2} \frac{k_n}{k_{n'}} \sum_{i=1}^N \Phi_{n,n'}^{(i)} \right] g_{\perp,n}^0(s) g_{\perp,n'}^0(s) - \frac{\beta}{2} \sum_{i=1}^N \Phi_{n,n'}^{(i)} g_{z,n}^0(s) g_{z,n'}^0(s) \right\}, \quad (\text{B9})$$

where

$$\Lambda_{n,n'} = \sum_{i=1}^N \frac{1}{2k_{n'}} \frac{k_n}{k_{\perp,n}^2} l (e_{z,n} h_{z,n'} - h_{z,n} e_{z,n'}) \Big|_{R_{i-1}}^{R_i},$$

with $k_{\perp,n}^2 = (\epsilon_i \mu_i \beta^2 - 1) k_n^2$. It can be seen that $\Lambda_{n,n'}$ is anti-symmetric upon the interchange ($n \leftrightarrow n'$), but that $\Lambda_{n,n'}$ is multiplied by quantities that are symmetric with respect to this interchange. Thus the first term in Eq. (B9) vanishes upon summation over n and n' . If one now invokes the orthonormalization relation [Eq. (2.11)], Eq. (B9) then becomes simply

$$\bar{P}_z = -v q_0 e \sum_{l=-\infty}^{\infty} \sum_{n=1}^{\infty} \frac{e_{z,n}^2(r_0)}{C_n} \Theta(-s), \quad (\text{B10})$$

since $g_{\perp,n}^2(s) + g_{z,n}^2(s) = \Theta(-s)$. It should be noted that the remarkably simple form of Eq. (B10) resulted even though no average was taken over either z or t . Radiated power \bar{P}_z is ‘‘naturally’’ independent of z and t . This, of course, is as it should be, since it results from the uniform drag on the charge bunch and therefore must itself be uniform. The minus sign in Eq. (B10) indicates that the radiated power flows in a direction opposite to that of the charge bunch, since the convected Coulomb field energy exceeds the Poynting flux.

-
- [1] T.-B. Zhang, J. L. Hirshfield, T. C. Marshall, and B. Hafizi, *Phys. Rev. E* **56**, 4647 (1997).
[2] W. Gai, P. Schoessow, B. Cole, R. Konecny, J. Norem, J. Rosenzweig, and J. Simpson, *Phys. Rev. Lett.* **61**, 2756 (1988).
[3] T. C. Marshall, T.-B. Zhang, and J. L. Hirshfield, in *Advanced Accelerator Concepts*, edited by Wes Lawson, Carol Bellamy, and Dorothea F. Brosils, AIP Conf. Proc. No. 472 (AIP, Woodbury, NY, 1999), pp. 27–37; T.-B. Zhang, T. C. Marshall, and J. L. Hirshfield, *IEEE Trans. Plasma Sci.* **26**, 787 (1998).
[4] M. Rosing and W. Gai, *Phys. Rev. D* **42**, 1829 (1990).
[5] K.-Y. Ng, *Phys. Rev. D* **42**, 1819 (1990).
[6] C. T. M. Chang and J. W. Dawson, *J. Appl. Phys.* **41**, 4493 (1970).
[7] J. G. Power, W. Gai, and P. Schoessow, *Phys. Rev. E* **60**, 6061

- (1999).
[8] W. K. H. Panofsky and W. A. Wenzel, *Rev. Sci. Instrum.* **27**, 967 (1956).
[9] P. B. Wilson, in *Physics of High Energy Accelerators*, edited by R. A. Carrigan, F. R. Huson, and M. Math, AIP Conf. Proc. No. 87 (AIP, New York, 1982), p. 450.
[10] J. L. Hirshfield, S. Y. Park, and T.-B. Zhang, in *Advanced Accelerator Concepts* (Ref. [3]), pp. 668–675.
[11] H. P. Freund and A. K. Ganguly, *Phys. Fluids B* **2**, 2506 (1990).
[12] R. E. Collin, *Field Theory of Guided Waves* (IEEE Press, New York, 1991), pp. 416–419.
[13] B. M. Bolotovskii, *Usp. Fiz. Nauk* **75**, 295 19961 [*Sov. Phys. Usp.* **4**, 781 (1962)].